COMPLEXATION OF METAL IONS IN AQUEOUS SOLUTION BY FLUORESCENT LIGANDS CONTAINING PYRIDYL GROUPS

Karen Anna Martha Oscarson

Department of Chemistry

University of North Carolina at Wilmington

2004

INTRODUCTION

Planck's quantum theory postulates that all atoms and molecules have discrete, quantized energy states. Electronic states originate from the motion of electrons around their respective nuclei. Vibrational states relate to the vibrational tendencies of molecules. Molecular rotational states derive from the revolving of molecules about their centers of gravity. When a molecule absorbs a quantum of electromagnetic radiation, promotion to a higher quantized energy level occurs. This increase in energy results in an energetically unfavorable excited state for the molecule. The excited state is relatively short-lived at room temperature, and, in accordance with the First Law of Thermodynamics, the molecule must emit an equivalent amount of energy when returning back to the ground state. This can occur via various emissive pathways, or a combination of two or more pathways. The energy diagram shown below in Figure 1 illustrates the possible routes of emission.

There are two types of excited electronic states. The excited singlet state arises when the spin paired electrons in an orbital in the ground state retain their spin paired orientation after one of the electrons is promoted into the higher energy level excited state by absorption of energy. This state is higher in energy than the excited triplet state, in which one of the electrons from the ground state pair is promoted to an excited singlet state, followed by intersystem crossing to the triplet excited state, with loss of the pairing between them. Photoluminescence emission describes the energy pathways by which light energy is emitted as the excited state molecular complex relaxes back to the preferred ground state. Phosphorescence is the most common photoluminescent pathway

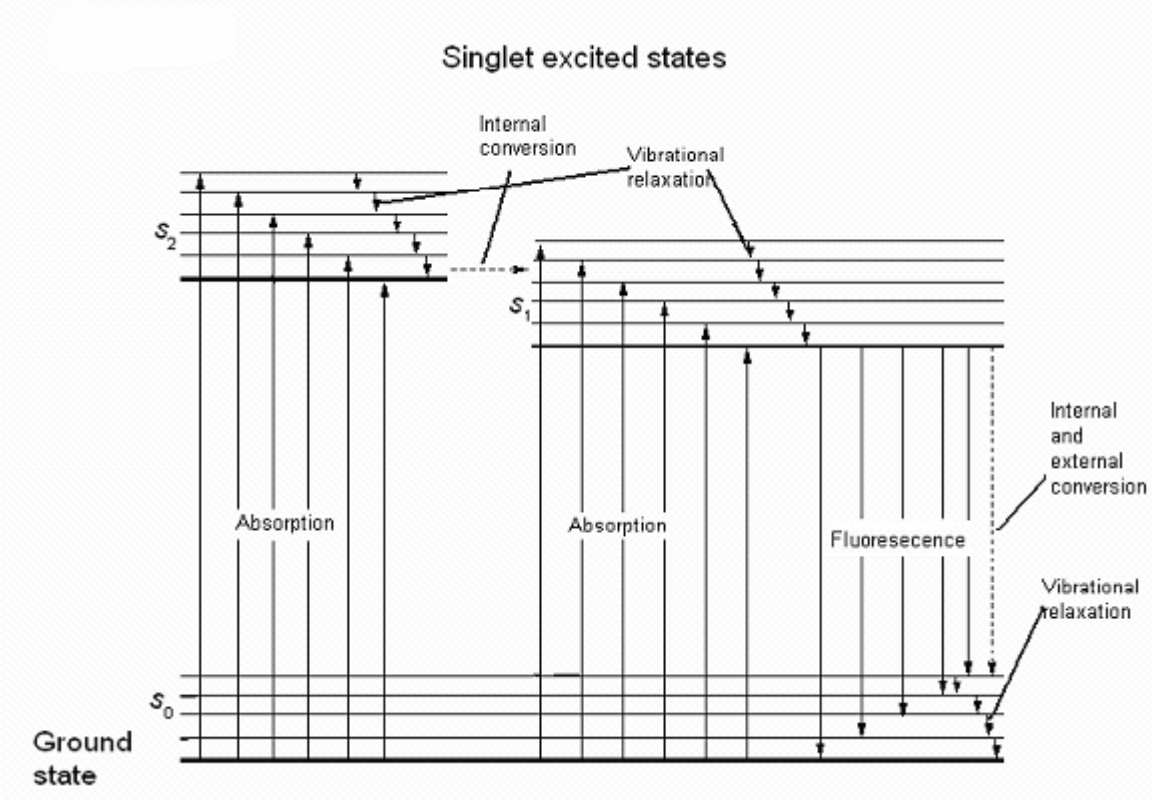

Figure-1.[1] Partial energy Jablonski diagram for a photoluminescent system (excited singlet state).

for the excited triplet state. Fluorescence arises from the singlet excited state complex. Because phosphorescence involves a change in electron spin, it is long-lived ($>>10^{-4}$) compared to fluorescence ($<10^{-5}$). The change in electron spin state involved in photoluminescence is spin-forbidden, accounting for the long-lived excited state.[1] The essential distinction is that, in fluorescence emission ceases when the source of excitation is removed, whereas in phosphorescence emission can occur for some time after the excitation source is removed.

Deactivation (returning to the ground state) extends to other types of processes besides those which emit a photon of radiation. These pathways are usually more efficient, and therefore "compete" with photoluminescent processes.[1] When vibrational relaxation occurs, the excited complex is promoted to a higher vibrational energy level which is ultimately lost to intermolecular collisions between the complex and solvent in solution[1]. Another process that is not well understood is internal conversion, which occurs when the excited-state complex goes to a lower energy electronic state without emission of a photon. Internal conversion describes a radiationless transfer between two electronic levels that are equivalent to each other in energy. The overlapping vibrational levels that result from the former equivalence provide a pathway for internal conversion, as shown in Figure 1 in the S2 to S1 transition.[1] Quenching competes with both deactivation and luminescence, as shown in the example below for quenching of a fluorophore D by molecular oxygen.[2]

$D + h\nu \rightarrow D^*$ excitation

$D^* \rightarrow D + h\nu$ or Δ luminescence or deactivation

$D^* + O_2 \rightarrow D + {}^*{}^1O_2$ quenching

Lone pairs of electrons can quench fluorescence[3] by formation of an exciplex between the π-system of the fluorescing group and the lone pair on, for example, an amine. An *exciplex* is an electronically excited complex of definite stoichiometry that is non-bonding in the ground state.

One precursor to quenching involves the static mechanism of ion-pairing which is dependent on interatomic distance between cation and anion. As the Lewis basicity of the anion adjacent to the fluorescent complex increases, the probability of quenching increases.[6] Another mechanism for quenching is dynamic collisional quenching, which is best described by the Stern-Volmer equation:

$$F_0 / F = 1 + K_D[Q] \qquad [1]$$

The F_0 / F ratio is the fluorescence intensity in the absence (F_0) and presence (F) of quencher. K_D is a quenching constant, while [Q] is the quencher concentration. This equation shows that, as more quencher is added to the solution, the fluorescence intensity of the complex diminishes.[3]

In a metal-ligand complex, charge transfer occurs when the electron promoted to form the excited state complex originates from the metal (metal to ligand charge-transfer, MLCT) or from the ligand (ligand to metal charge-transfer, LMCT).[4] The former is the most common charge-transfer type. More difficult to characterize are the metal to metal (MMCT) and the metal to solvent (MSCT) excited states. Fluorescence most commonly occurs from electronic transitions between $\pi^* \rightarrow \pi$ lower-lying energy levels.[1] As conjugation is known to lower the overall molecular energy[5], and so decrease the energy gap between the π^* and π system, highly conjugated aromatic compounds fluoresce more readily when excited.

The energy gap law can be useful in predicting nonradiative rate constant behavior for metal-ligand complexes, though radiative decay is independent of the nature of the ligand.[6] The law states that the emission energy (i.e. energy gap) of an excited-state complex is inversely proportional to the nonradiative decay rate. Fluorescence quantum yield (Q) is dictated by the following equation:

$$Q = [\ \Gamma / (\Gamma + k_{nr}\ )] \qquad [2]$$

Where Γ is the radiative decay rate and k_{nr} is the nonradiative decay rate. As the value of k_{nr} increases, the emission energy diminishes.

Solvent effects can be seen in excited state metal-ligand complexes. Generally, increasing polarizability of a solvent leads to increasing hypsochromic shifts in the emission spectra.[6]

Fluorescence can be enhanced by increasing structural rigidity of a molecule.[1] Structural rigidity refers to the physical constraints of a molecule (Figure 2a). A polyaromatic such as phenanthrene fluoresces more intensely than does 1,4-diphenylbenzene because it has fewer rotational and vibrational degrees of freedom. The latter limits the competing vibrational paths of relaxation. In addition, if the molecular geometry of the excited state is different from that of the ground state, the Franck-Condon principle prevents the electron from returning to the ground state. The Franck-Condon principle states that electronic motion is much faster than the motion of atomic nuclei. The effect of this is that if the structure of a metal complex in two oxidation states is fairly different, then electron transfer between the two oxidation states becomes difficult. An example of this is that electron transfer between $[Co(NH_3)_6]^{3+}$ and

$[Co(NH_3)_6]^{2+}$ is very slow, since the Co-N bond lengths in low-spin Co(III) complexes are much shorter than those in high-spin Co(II) complexes.

An example of the effect of the Franck-Condon principle regarding photoluminescence is the Cu(I) complex of 1,10-phenanthroline (1,10-phen).[7] On excitation of the ground state complex of Cu(I), an electron is excited out of the e_g level to the π* level of the ligand. The complex has effectively become one of Cu(II) with a free radical 1,10-phen$^-$ coordinated to it. Cu(I) prefers to be tetrahedral, and Cu(II) prefers to be square planar. Thus, while the electron in the excited state is in the π* –system of the ligand, the geometry around the 'Cu(II)' distorts towards square planar. In this state the Franck-Condon principle dictates that the electron cannot fall directly back into the e_g level of the 'Cu(II)', so that fluorescence does not occur. The molecular geometry of Cu(I) 1,10 phenanthroline complexes has been studied computationally[8] (Hartree-Fock) and found to exhibit a "flattening" during excitation, which ultimately contributes to a shorter fluorescence lifetime[9]. Addition of bulky substituents in the 2 and 9 positions of the 1,10-phen ligand to give the ligand neocuproine hinders this flattening, so that fluorescence is strong in the Cu(I)/bis-neocuproine complex.[9]

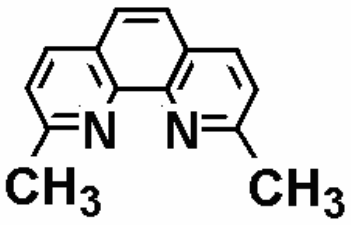

neocuproine

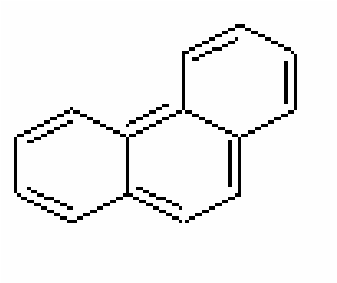

phenanthrene

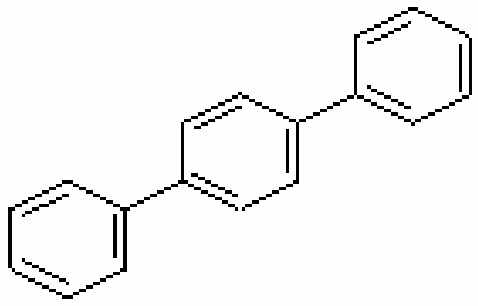

1,4-diphenylbenzene

Figure 2(a). Phenanthrene has more structural rigidity than does 1,4-diphenylbenzene; at each carbon-carbon bond, the former has fewer opportunities to relax via vibrational or rotational pathways than does the latter.

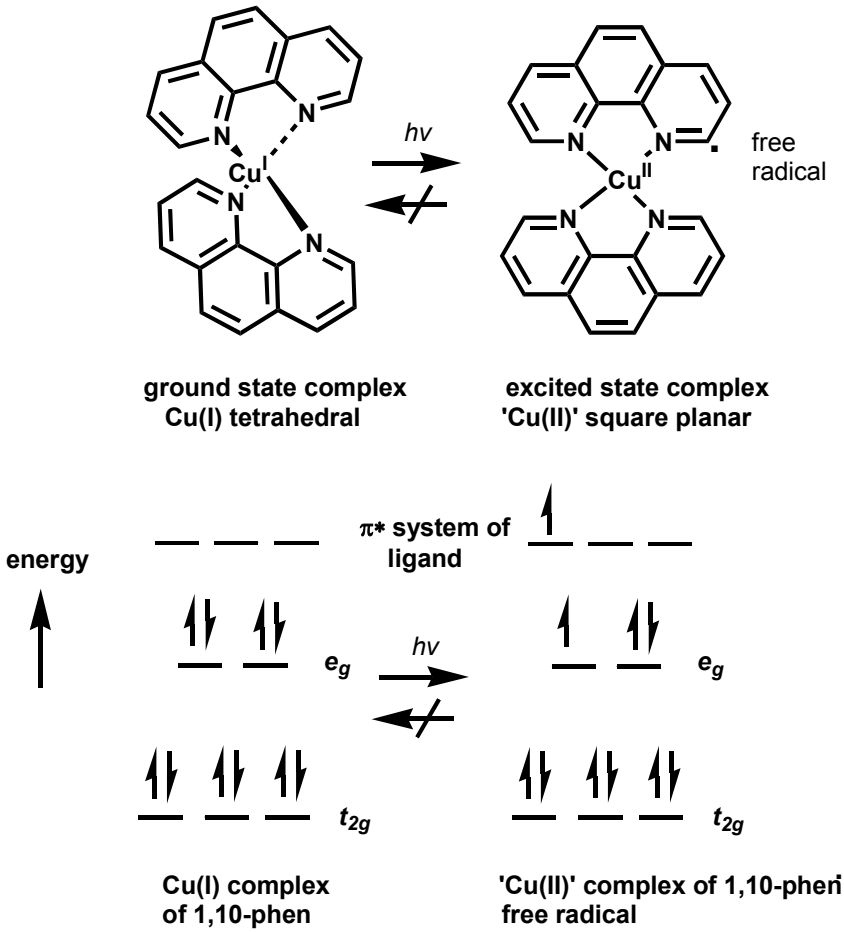

Figure 2(b). Excitation of an electron in the $[Cu(1,10\text{-phen})_2]^+$ complex (left), which is tetrahedral in the ground state, to the excited state (right). In the excited state the excited electron comes from the e_g level of the ground state, thus effectively oxidizing Cu(I) to 'Cu(II)'. At the same time one of the 1,10-phen ligands becomes a free radical, indicated as 1,10-phen·. The Franck-Condon principle prevents the electron from falling back into the ground state since the complex has moved towards being square planar 'Cu(II)'. Note that the electron in the excited state has, after intersystem crossing, become non-spin paired with respect to the unpaired electron left in the e_g level, so that this process is phosphorescence rather than fluorescence, and one expects a long-lived excited state.

Fluorescence is well established for Ca(II) and Zn(II)[10-13] complexed with ligands with fluorophores attached. It is not clear that photon emission generally will or will not occur for metal ions with partially filled *d*-shells. What is clear is that the paramagnetic metal ions Cu(II) and Ni(II) (d^9 and d^8 metal ions) quench fluorescence very strongly.[14] On the other hand, photoluminescence of complexes of Ru(II) (low-spin d^6) with unsaturated ligands such as 2,2'bipyridyl is well established.[15] As shown in Figure 3, for photoluminescence to occur, the relationship between the S_o ground state and the excited state must be correct. The S_o ground state for $[M(bipy)_3]^{2+}$ complexes (M = Fe, Ru, Os) is the t_{2g} level. The excited state refers to the π* orbitals of the ligand. The e_g* level must be higher in energy than the π* level of the ligand, or quenching will occur. Thus, for M = Fe(II), photoluminescence does not occur because the e_g* level (Figure 3) is lower in energy than the π* level. For M = Ru(II), the reverse is true, and a strong emission occurs. For M = Os(II), the e_g level is much higher than the π* level, so quenching does not arise from this source. However, the gap between the ground state (S_o) t_{2g} and excited state π* levels has now become too small. According to the energy gap law, as the energy of the excited state becomes closer to the ground state, the rate of radiationless decay increases.[15] Thus, the Os(II)/ tris-bipyridine complex phosphoresces only weakly, and that occurs at very long wavelengths. Luminescent Os(II)/ ligand complexes typically have long-wavelength emission, a low-energy MLCT state, and a rapid rate of radiationless decay.

The implications of the energy gap law here for metal ions such as Ni(II) are not at this point clear. In Zn(II) complexes, which are generally excellent for

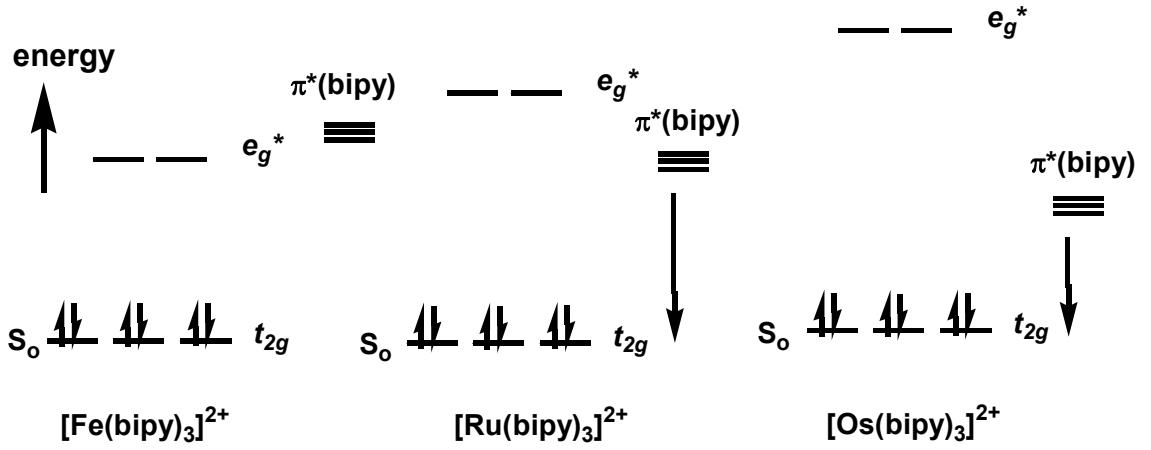

Figure 3. The energy levels of tris-bipy complexes of low-spin divalent d^6 metal ions, $[M(bipy)_3]^{2+}$, where M = Fe(II), Ru(II) or Os(II). Note that for phosphorescence to be observed, the e_g* level should be higher in energy than the π* level of bipy, or quenching will occur. Thus $[Fe(bipy)_3]^{2+}$ is not phosphorescent. The Ru(II) complex has the e_g* level higher in energy than the π* level, and so is strongly phosphorescent. The Os(II) complex has the energy gap between the e_g* and π* level very large, so this does not contribute to quenching. However, the π* level is now rather close to the t_{2g} level, and so, according to the energy gap law, which states that as the energy of the excited state becomes closer to that of the ground state (S_o), the rate of radiationless decay increases. Thus, the Os(II) complex is only weakly phosphorescent, and at long wavelengths because of the small energy gap between the π* and t_{2g} levels.

photoluminescence, the e_g* level is close in energy to the π* level of the ligand, but is filled, and so does not lead to quenching. Complexes of high-spin Ni(II) are powerful quenchers of photoluminescence. This probably involves electron transfer from the π* excited state of the ligand to the partly filled e_g* level of the Ni(II) (Figure 4). The question here is whether the formation of a square planar low-spin complex would raise the energy of the d_{x2-y2}* level above the π* level of the ligand (Figures 4 and 5), in this case terpyridine (terpy). If this did not occur, then photoluminescence would be quenched. However, if the Ligand Field (LF) strength of the attached ligands is high enough to raise the energy of the d_{x2-y2}* level above the π* level of the ligand (Figure 4), in this case terpy, then photoluminescence would be possible. An aim of this work is to see whether equilibria such as the one below would produce low-spin fluorescent complexes:

$$[Ni(terpy)(H_2O)_3]^{2+} + CN^- \leftrightarrows [Ni(terpy)CN]^+ + 3H_2O$$

high-spin — low-spin

non-fluorescent — fluorescent

(?)

The Chelation Enhanced Fluorescence (CHEF) Effect

The fluorescence of aromatic molecules such as anthracene can be quenched by the presence of bases with lone pairs capable of forming an exciplex with the excited state of the aromatic system.[10-13] Thus, molecules such as 1,10-phenanthroline (1,10-phen) fluoresce only weakly, because the lone pairs that they bear quench their fluorescence. However, when the ligand forms a complex with a suitable metal ion, the lone pairs of the ligand are now involved in bond formation with the metal ion, and fluorescence is

greatly enhanced. This is referred to as the Chelation Enhanced Fluorescence (CHEF) effect. The complexes of metal ions such as Zn(II), Ca(II), or Ru(II), discussed in this work, all exhibit the CHEF effect, in that the fluorescence of attached ligands such as 1,10-phen is greatly enhanced by complex-formation with these metal ions. The proton is also able to enhance fluorescence by binding to the lone-pairs of the ligand. To cause a CHEF effect, the metal ion should not only bind to the ligand, but also meet the requirements of the Energy Gap Law, as well as have correct energies for the e_g levels relative to the π^* levels of the aromatic system, as discussed above. The CHEF effect is of considerable importance, in that it forms the basis for the determination of the location of concentrations of Ca^{2+} in studies of the living cell.[10-13] An important ligand for this type of application has been FURA-2 (see below for the structure of FURA-2). The lone pairs on oxygen and nitrogen donor atoms of FURA-2 quench the fluorescence of the molecule, but when Ca^{2+} coordinates, a strong CHEF effect is observed.[10-13] The CHEF effect is of considerable importance in this study in relation to complexes of Ni(II) with terpyridine, In(III) with 1,10-phen, and a variety of metal ions with FURA-2 itself.

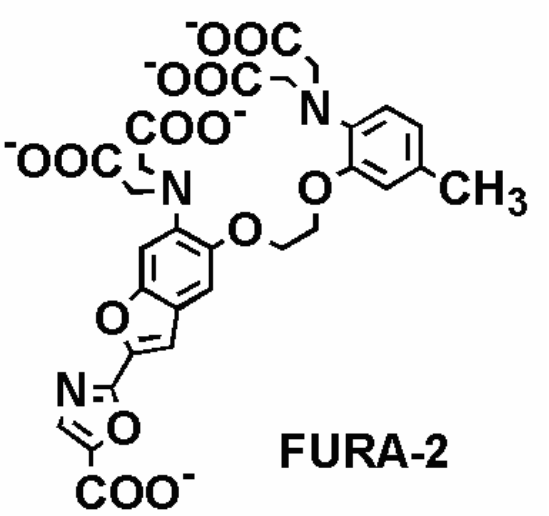

FURA-2

Ligand Design Rules

This research is concerned with assessing trends seen with the N-donor aromatic ligands n-terpyridine, 1,10-phen, and neocuproine. Ligand design rules developed by Hancock *et al.,*[16-18] were implemented when the experiments were planned.

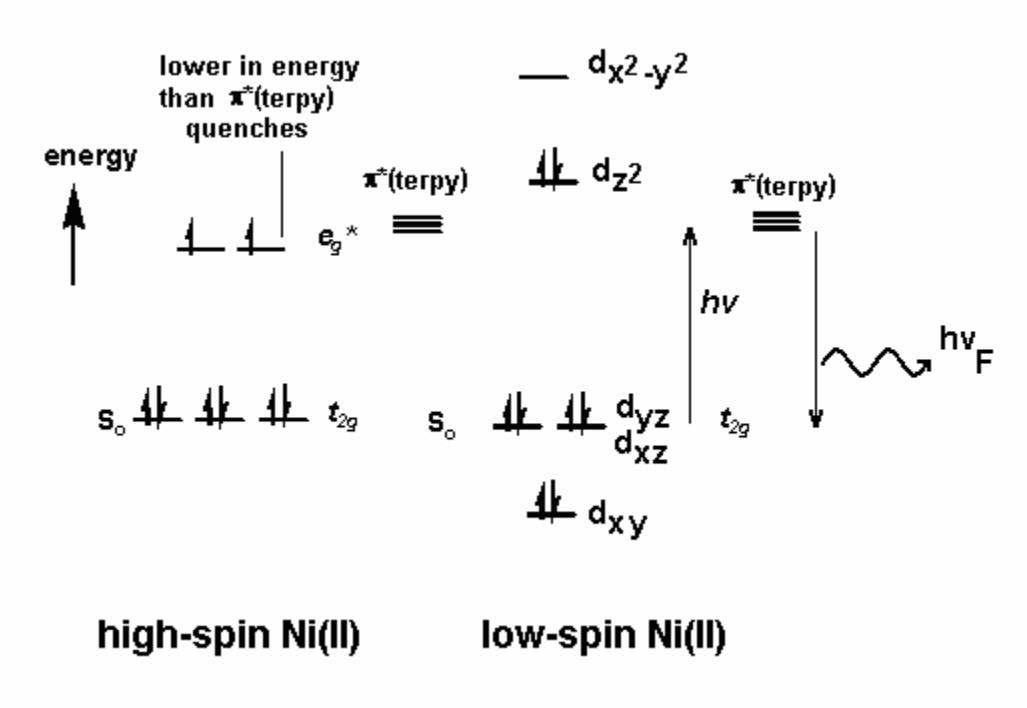

Figure 4. Energy levels in Ni(II) complexes, and how adopting a low-spin state for Ni(II) may remove the partly filled e_g* levels that lead to quenching of the excited state of the * orbitals of a ligand such as terpy.

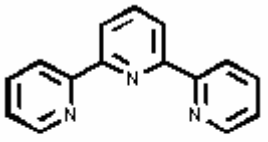

n-terpyridine

(terpy)

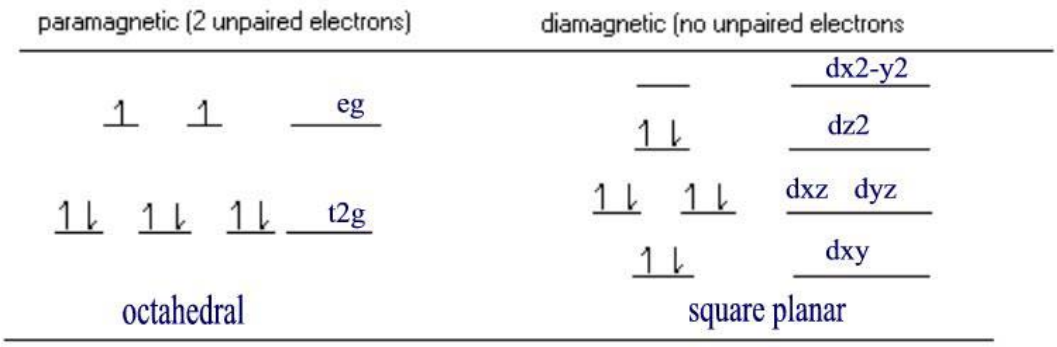

Figure 5. The possible spin states and resulting geometries for nickel (II) complexes. Ni(II) has 8 available d-electrons for bonding.

Two factors are important in ligand design rules.

Metal Ion Size: One is the size of the metal ion. Different sizes of chelate rings favor different sizes of metal ions. Thus Ni^{2+}, In^{3+}, Cu^{2+}, Zn^{2+}, and Cd^{2+} were selected in this research to show the selectivity of the ligands designed for Zn^{2+}, because the radius (r^{+}) of these metal ions range in order from small (Ni^{2+}, r^{+} = 0.67 Å) to large (Pb^{2+}, r^{+} = 1.19 Å). This provides the basis for demonstrating how the sensors can increase the selectivity for Zn^{2+} when one of the chelating ring changes from the five membered to six membered ring size.

Chelating ligands are compounds with more than one donor atom, which can form chelate rings when they form coordination complexes with metal ions. Unidentate ligands have one donor atom, such as $(CH_3)_3N$, OH^{-}, F^{-}. The increased stability produced when chelating ligands form coordination complexes with metal ions compared with those of unidentate analogs is known as the chelate effect. This is seen for the formation constants of the complexes of Ni^{2+} with *n*-dentate polyamines, as compared with the analogous complexes with ammonia (shown in Table-1[19]).

Nature of the donor atom

Pearson's HSAB (hard and soft acid and base) model is a method of prediction of stable metal-ligand complex formation.[16] Pearson states that hard acids complex preferably with hard bases and soft acids prefer to bind with soft bases. Hard acids include the Group I and II A metals (H^{+} also) as well as the lighter transition metals in high oxidation states (see Table 2). Hard bases extend to oxygen- and nitrogen-containing ligands (see Table 3). Borderline acids and bases can readily complex with either hard or soft compounds.

Table-1.[19] The chelate effect for complexes of Ni(II) with polyamines.

polyamine	EN	DIEN	TRIEN	TETREN	PENTEN
denticity, n	2	3	4	5	6
log β_n (NH_3)	5.08	6.85	8.12	8.93	9.08
log K_1 (polyamine)	7.47	10.7	14.4	17.4	19.1

Where:
Ionic strength = 0.5 M
EN $NH_2CH_2CH_2NH_2$
DIEN $NH_2(CH_2CH_2NH)_2H$
TRIEN $NH_2(CH_2CH_2NH)_3H$
TETREN $NH_2(CH_2CH_2NH)_4H$
PENTEN $NH_2(CH_2CH_2NH)_5H$
$\log \beta_n(NH_3) = \log(K_1 \times K_2 \text{ ----- } \times K_n)$
Note that the chelate effect increases with the increase of denticity.

Table 2a. Pearson's *Hard* Lewis Acids.

H^+	Na^+	K^+	Be^{2+}	Mg^{2+}
Ca^{2+}	Mo^{3+}	Mn^{2+}	Al^{3+}	Sc^{3+}
In^{3+}	Cr^{3+}	Co^{3+}	Fe^{3+}	Ti^{4+}
Zr^{4+}	U^{4+}	Ce^{3+}	Sn^{4+}	BF_3
$AlCl_3$	AlH_3	SO_3	NO_2^+	CO_2

Table 2b. Pearson's *Borderline* Lewis Acids.

Fe^{2+}	Co^{2+}	Ni^{2+}	Cu^{2+}	Zn^{2+}
Pb^{2+}	Sn^{2+}	Sb^{3+}	Bi^{3+}	Ir^{3+}
$B(CH_3)_3$	SO_2	Ru^{2+}	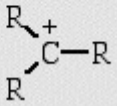	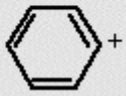

Table 2c. Pearson's *Soft* Lewis Acids.

Cu^+	Ag^+	Au^+	Tl^+	Hg_2^{2+}
Pd^{2+}	Cd^{2+}	Pt^{2+}	Hg^{2+}	Tl^{3+}
BH_3	Br^+ I^+	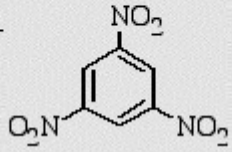	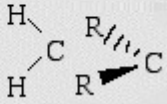	$R-S^+$
$R-Se^+$	Br_2 I_2			$H-O^+$

Table 3a. Pearson's *Hard* Lewis Bases.

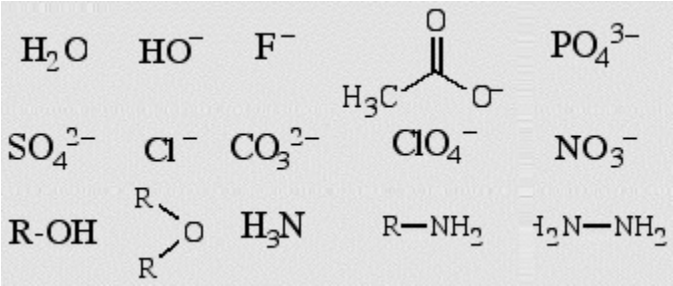

Table 3b. Pearson's *Borderline* Lewis Bases.

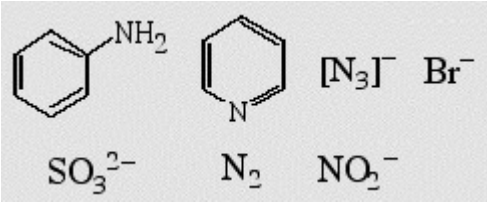

Table 3c. Pearson's *Soft* Lewis Bases.

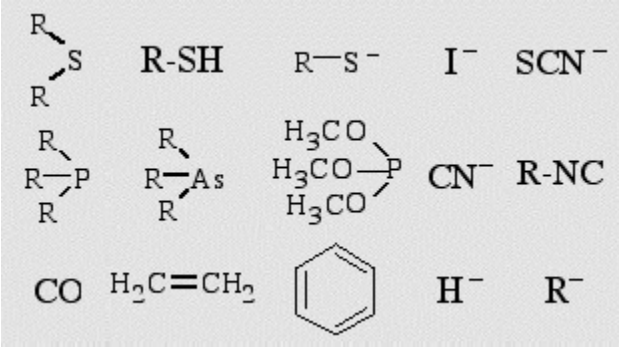

Voltammetry

Voltammetry is an electrochemical technique in which an applied potential is used to generate a current, and polarization is facilitated by the small surface area of a microelectrode. The microelectrode in voltammetry is a dropping mercury electrode (DME), whose drop size is reproducible and whose rate can be controlled. Differential pulse voltammetry offers better peak resolution and a higher Faradaic current to charging current ratio by considering the change in current at the beginning and end of a pulse superimposed on a linearly increasing voltage[1]. An advantage of differential pulse voltammetry is the detectability of the analyte at low concentrations [10^{-6} *M*]. This allows for chemical species that are relatively insoluble in aqueous media to be studied. The following simplified equation[22] relates maximum peak current, Δi_{max}, to concentration of the analyte (C):

$$\Delta i_{max} = (n2F2/4RT)AC(-\Delta E)\text{-}(D/\pi t_m)^{1/2} \qquad (3)$$

Where (A) is the area of the electrode, ΔE is the voltage pulse , t_m is the time between the pulse and current measurement, (*D*) is the analyte diffusion coefficient, and (*n*) equals the number of electrons.

Metal- ligand complex formation and equilibrium can be studied in solution. Two distinct behaviors of analyte solutions can arise as a result of applied voltammetric waves. The free ligand and free metal species, along with the metal-ligand complex, can come to equilibrium at the electrode surface faster than the voltammetric time-scale can detect. This is known as a labile system. In a labile system, the formation constant (K_f) for the complex can be determined using the Lingane equation:

$$(E_{1/2})_C - E_{1/2} \leftrightarrow -\frac{0.0592}{n} \log K_f - \frac{0.0592x}{n} \log C_L \qquad (4)$$

In the Lingane equation, $(E_{1/2})_C$ is the half-wave potential for the complexed species and $E_{1/2}$ is for the uncomplexed species.

A non-labile system occurs when the rate of equilibrium for the analyte is slower than the reduction by the voltammetric process. For non-labile systems, the diffusion coefficient of each of the species can be obtained from the peak height corresponding to each voltammetrically active species in solution.

The pK_a values of terpyridine, 1,10-phen, and neocuproine can be determined by collecting data sets of peak potential (E) as a function of both the volume of titrant added, and the resulting pH under voltammetric conditions. The standard potential $E°$ and a Nernstian slope can be calculated and determined in an acid-base titration. From this data it is possible to calculate values of $\overline{n}$, the number of protons bound per ligand molecule in solution. From an $\overline{n}$ versus pH curve, one can calculate the pK_as of the ligand.

Nuclear Magnetic Resonance Spectroscopy in the study of solution equilibria.

The most common NMR nucleus used for analysis[23] is ^{1}H. ^{1}H NMR can be used to provide information regarding metal-ligand complex behavior as a function of pH. An NMR-based method was used to confirm the values of the In-1,10 phenanthroline complex initially obtained from differential-pulse voltammetry.

The objectives of this study were:

1) To examine the distribution of metal ions in the Periodic Table that are able to induce photoluminescence on formation of complexes. Particular questions would be that if Zn(II) always induces a CHEF effect, would iso-electronic ions such as In(III) be able to?

2) It turned out that In(III) did weakly induce fluorescence in complexes with ligands such as 1,10-phen, where Zn(II) induced strong fluorescence. The affinity of In(III) with nitrogen-donor ligands is poorly established, so that a part of this study was devoted to determining whether the In(III) was actually forming a complex with 1,10-phen. Techniques used in this study were voltammetry and NMR.

3) High-spin Ni(II) appears to quench fluorescence on coordinating to ligands bearing fluorophores. Would a change to low-spin Ni(II) allow for fluorescence, or would problems such as inappropriate energies for the resulting metal ion orbitals still lead to problems as with the energy-gap law.

EXPERIMENTAL

General

Materials: Methanol was purchased from VWR, ethanol from AAPER, and acetone was obtained from Fisher, while deuterium oxide 99.9% (with 1% w/w DSS) was purchased from Aldrich. Milli-Q® (MQ) water was processed in-house. N-terpyridine 98% and neocuproine 99% were procured from Aldrich. 1,10-phen monohydrate 99.8% crystals were obtained from Baker. Zinc perchlorate hexahydrate 99%, nickel(II) nitrate hexahydrate 99.999%, copper(II) perchlorate hexahydrate 98.9%, indium(III) nitrate hydrate 99.9%, lead nitrate 99.99%, and sodium perchlorate 99% were purchased from Aldrich. Sodium nitrate 99.99% was obtained from Fisher. 1.000 *M* and 0.0975 *M* nitric acid were purchased from Acros. Sodium hydroxide 10.00 $\pm$0.05 N solution was purchased from VWR. Copper(I) tetraacetonitrilotetrafluorophosphate was a gift from Curtis M. Whaley.

The physical techniques used in this research were fluorimetry, voltammetry, NMR spectroscopy, and FT-IR. Hyperchem was utilized for molecular modeling.[24]

^{1}H NMR experiments were performed using a Bruker 400 MHz Avance DRX spectrometer. A VWR SR601C pH meter was used for potentiometry, as well as for monitoring pH during voltammetry, fluorescence, and NMR experiments. A Mattson Polaris™ was used for FTIR spectroscopic evaluation. A Metrohm 663 VA stand was coupled with an Ecochemie PGSTAT10 potentiostat and Ecochemie General Purpose Electrochemical System (GPES) Software for voltammetry experiments. Fluorescence experiments were carried out with a Fluoromax-3™ and a Shimadzu RF-551.

The three areas that represented the main crux of the research reported here, along with the techniques used, can be summarized as the following:

a. Possible induction of fluorescence of the Ni-terpyridine complex by secondary ligands and as a function of pH. FURA-2 was used as a positive control for CHEF effect with $Ca^{2+}$and Zn^{2+}; Ni^{2+} quenched fluorescence with FURA-2. Also, addition of secondary ligands that may cause a change of spin-state of the Ni(II) on binding to the Ni(II)-terpyridine complex. Zn(II)-terpyridine was used as a positive control in this case. Voltammetry was used to determine pKa of Ni(II)-terpyridine to further characterize its behavior in aqueous solution.
b. Using fluorimetry to study selective fluorescence of Cu(I) that occurs with neocuproine, but not with 1,10-phen.
c. Determination of the binding constant for indium with 1,10-phen by voltammetry, and verification of this constant by ^{1}H NMR. The interest here was whether a metal ion such as In(III), which is isoelectronic with Zn(II) and Cd(II), would produce strong CHEF effects when complexed with a fluorophore. The question that arose with the 1,10-phen complex was whether its lack of a CHEF effect with In(III) was due to it not forming under the conditions of the experiment.

The protonation constants of *n*-terpyridine, neocuproine, and 1,10-phen were obtained from the NIST database[25]. The pK_a of the Ni(II) complex of terpyridine was determined by collecting data sets of the voltammetric potential (E) as a function of the measured pH in sets of acid-base titrations in a voltammetric titration cell. The standard potential for the cell (glass electrode plus reference electrode), $E°$, and a Nernstian slope were calculated from separate acid-base titrations.

Preparation of stock solutions

Terpyridine stock solutions: 0.45 g terpyridine (FW = 234.3 g/mol) was added to ~20 mL MQ H_2O in a 25.0 mL volumetric flask to make up a 0.076 *M* solution. 3.0 mL of 1.00 *M* nitric acid were added prior to filling to the mark to ensure that the terpyridine was completely dissolved. The solution was stored in the dark and a fresh stock solution was made up weekly. Dilutions were made as needed.

Nickel chloride pentahydrate: 1.81 g Ni(II) chloride pentahydrate were dissolved in 100 mL MQ H_2O in a 100 mL volumetric flask.

Zinc perchlorate hexahydrate: 2.83 g Zn(II) perchlorate hexahydrate were dissolved in 100 mL MQ H_2O in a 100 mL volumetric flask.

FURA-2: A pre-weighed 1 mg amount of FURA-2 tetrasodium salt was charged to a 1.00 L volumetric; filled to mark with MQ H_2O. The stock solution was stored in the dark until use.

Calcium perchlorate: 0.31 g $Ca(ClO_4)$ $4H_2O$ was dissolved in a 100 mL volumetric flask and made up to the mark with MQ H_2O.

Copper perchlorate: 0.37 g $Cu(ClO_4)$ $6H_2O$ was dissolved in a 100 mL volumetric and filled to the mark with MQ H_2O.

Sodium cyanide: 0.019 g NaCN was placed in a 15 mL flint vial, and 10.0 mL MQ H_2O was added to the vial. The resulting solution was sonicated until the NaCN dissolved.

Sodium hydroxide: A stock solution of 10.00 $\pm$0.05 *M* NaOH solution was diluted as needed to provide solutions that were typically 0.01 *M*, which were standardized by acid-base titration with standard acid.

Pyridine: A 0.25 *M* pyridine stock solution was made by diluting 2.04 mL pyridine in with MQ H_2O in a 100 mL volumetric flask.

Sodium azide: A 0.25 *M* sodium azide stock solution was made by dissolving 0.8125 g sodium azide in MQ H_2O, in a 50 mL volumetric flask.

Nickel-terpyridine: A nickel-terpyridine stock solution for voltammetric use was made by dissolving 0.058 g of terpyridine in a 50 mL volumetric flask, followed by addition of about 10 mL MQ H_2O. 2 mL of 1.00 *M* HNO_3 was added to increase solubility. 0.059 g $NiCl_2 \cdot 6H_2O$ was then added to the flask, and MQ H_2O was used to make the solution up to the mark. The resulting solution was sonicated for 15 minutes.

1.0M $NaNO_3$: 42.5 g of $NaNO_3$ was weighed into a 500 mL volumetric flask, and MQ H_2O was added to the mark.

0.01M NaOH in 0.49M $NaNO_3$: 1.00 mL of 1.0 *M* NaOH and 49.0 mL of 1.0 *M* $NaNO_3$ stock solution were added to a 100 mL volumetric flask and MQ H_2O was added to the mark.

0.001M NaOH in 0.499M $NaNO_3$: 100 µL of 1.0 *M* NaOH and 49.9 mL of 1.0 *M* $NaNO_3$ were added to a 100 mL volumetric flask, and made to the mark with MQ H_2O.

0.01 M HNO_3 in 0.49 M $NaNO_3$: 1.00 mL of 1.00 *M* HNO_3 and 49.0 mL of 1.0 M $NaNO_3$ were charged to a 100 mL volumetric, and made to the mark with MQ H_2O.

Zinc-terpyridine: A zinc-terpyridine stock solution for voltammetric use was made by placing 0.059 g of terpyridine in a 50 mL volumetric flask, followed by about 10 mL MQ H_2O. 10 mL of 1.00 *M* HNO_3 was then added to aid in dissolving the terpyridine. 0.093 g $ZnClO_4 \cdot 6H_2O$ was added to the flask, and MQ H_2O was filled to the mark, and the flask was sonicated for 5 minutes.

Terpyridine in 0.1 M HNO_3 + 0.4 M $NaNO_3$: 0.012 g terpyridine was charged to a 100 mL volumetric flask; 10.0 mL 1.00 *M* HNO_3 was added to the terpyridine. Sonication was performed for five minutes. The volumetric flask was then made up to the mark with the 1.0 *M* $NaNO_3$ stock solution.

0.0095 M terpyridine: 0.1108 g terpyridine was weighed into a 50 mL volumetric flask and 2.00 mL of 1.00 *M* HNO_3 were added. MQ H_2O was then added to fill to the 50 mL line and resulting solution was sonicated for 5 minutes.

Cu_2O-terpyridine: Weighed 0.017 g Cu_2O and added to a 25 mL volumetric flask. Added 0.0095 M terpyridine stock solution to the flask, and sonicated for 10 minutes until dissolved.

1,10-phenanthroline: A 500 mL volumetric flask was charged with 0.0991 g 1,10-phen monohydrate crystals. 10.0 mL 1.00 *M* HNO_3 solution was then added to dissolve the 1,10-phen. Filled to the 500 mL mark with MQ H_2O to make a 0.001 *M* 1,10-phen solution, and stored the resulting solution in the dark until use.

Zinc(II) perchlorate: 0.932 g $ZnClO_4 \cdot 6H_2O$ was weighed into a 250 mL volumetric flask, and MQ H_2O was used to fill to the mark.

0.01 M Indium(III) solution: Add 0.98 g indium(III) nitrate hexahydrate to a 250 mL volumetric flask. The flask was then filled to the mark with MQ H_2O, and sonicated for 10 minutes to dissolve.

10^{-5} M Indium plus *10^{-4} M 1,10-phen* plus *0.01 M HNO_3* plus *0.09 M $NaNO_3$:* In a 500 mL volumetric flask, 0.101 g 1,10-phen and 5.00 mL 1.00 *M* HNO_3 were added. 3.825 g $NaNO_3$ was then weighed out and added to volumetric flask, along with 0.500 mL of 0.01 *M* In(III) stock solution. The flask was then filled to the mark with MQ H_2O.

5x10 $^{-3}$M $ZnNO_3$: Dissolved 0.149 g $Zn(NO_3)_2$ in MQ H_2O, in a 100 mL volumetric flask.

10 $^{-4}$M neocuproine: Dissolved 0.021 g neocuproine hydrochloride monohydrate in 5.00 mL of 1.000 *M* HNO_3 in a 1.00 L volumetric flask. The flask was then filled to the mark with MQ H_2O, and the resulting solution was stored in dark until use.

10 $^{-3}$M neocuproine: Dissolved 0.052 g neocuproine hydrochloride monohydrate in 10.00 mL of 1.000 *M* HNO_3 in a 250 mL volumetric flask. The flask was then filled to the mark with MQ H_2O, and the resulting solution was stored in dark until use.

1.0M $ZnNO_3$: Dissolved 14.9 g $ZnNO_3$ in MQ H_2O in a 50 mL volumetric flask.

1.0M SCN: Added 4.053 g sodium thiocyanate to a 50 mL volumetric flask, and dissolved with MQ H_2O.

10 $^{-3}$M 1,10-phen in 0.001 N HNO_3 + 0.099 N $NaNO_3$: Dissolved 0.099 g 1,10-phen monohydrate in 0.500 mL of 1.000 *M* HNO_3 in a 500 mL volumetric flask. Weighed 4.207 g $NaNO_3$ and added to volumetric flask. The flask was then filled to the mark with MQ H_2O, and the resulting solution was stored in dark until use.

Synthesis of complexes, and growth of crystals for crystallographic studies

$[Ni(terpy)_2][Ni(CN)_4]$: A 1:1:1 solution of Ni(II)-terpyridine-CN, each 0.0038 *M*, was prepared as followed: 0.15 g terpyridine was dissolved in 25 mL of acetone. In another beaker, 0.09 g $NiCl_2.6H_2O$ was dissolved in 25 mL ethanol and stirred to dissolve. In a separate beaker, 0.019 g NaCN was dissolved in 50 mL ethanol. The $NiCl_2.6H_2O$ and terpyridine solutions were combined, and allowed to stand for 24 hours to allow for the slow rate of complex-formation. NaCN solution was added 24 hours later, and allowed to stand in the dark with parafilm covering the beaker, with small holes in the parafilm to allow for slow evaporation.

$[Cd(neocuproine)(NCS)_2]_2$: A 1:1:2 solution of Cd(II)-neocuproine-SCN was prepared, each component being 0.0038 M. The following stock solutions were prepared initially:

$10^{-2}M\ CdClO_4$: 0.231 g $CdClO_4$ was added to a 100 mL volumetric flask, which was then filled to the mark with MQ H_2O.

$10^{-2}M$ neocuproine: 0.104 g neocuproine was added to a 100 mL volumetric flask; filled to mark with MQ H_2O.

$10^{-2}M$ SCN: 0.0825 g NaSCN was added to a 100 mL volumetric flask; filled to mark with MQ H_2O.

In a clean beaker, 10.0 mL $CdClO_4$ stock and 10.0 mL neocuproine stock solution were combined. Added 20.0 mL SCN stock 24 hours later; set aside in the dark with parafilm covering with holes pierced in the parafilm until solvent has evaporated.

Calibration of pH meter

For less precise work, the pH meter was calibrated using pH 2.00, 4.00, 7.00, and 10.00 buffer solutions (all $\pm$ 0.02 pH units at 25 °C). For work done at lower pH, only

pH 2.00, 4.00, and 7.00 buffer solutions were employed for calibration. For higher pH solutions, pH 4.00, 7.00, and 10.00 buffer solutions were used. For a broad pH range, pH 2.00, 7.00, and 10.00 buffer solutions were used. Each solution to be used for titration purposes was placed in a jacketed cell, with water flowing through the jacket from a thermostatted bath, which was set at 25.00 ± 0.05 °C. Calculated slopes >95% and <105% were deemed acceptable. If out of range, an electrode calibration was conducted and corrected pH values were generated.

Calibration of glass electrode

For more accurate work, acid - base titrations were carried out for calibration of the glass electrode system. A standard 1.000 *M* HNO_3 solution was used to prepare a 0.01 *M* HNO_3 secondary standard solution. The ionic strength of the solutions was kept constant at $I = 0.10$ with $NaNO_3$. A solution of 0.01 *M* NaOH concentration was also prepared from the 10.00 *M* standard NaOH solution, and standardized with the standard 0.01 *M* acid solution. 25 ml of the acid solution was placed in the temperature-controlled cell, which was preset to 25.00 ± 0.05 °C. Nitrogen gas was bubbled through the solution during titrations to exclude CO_2. The acid was titrated with 50 ml 0.01 *M* base, with 1 ml increments. The potentials were recorded on a VWR SR601C pH meter, reading to ±0.1 mV. The titration was used to standardize the 0.01 *M* NaOH from the midpoint of the curve of mV versus volume of base added (Figure-6a). From the known concentrations of the acid and base, the pH was calculated for each titration point. The standard potential ($E°$) and the experimental Nernstian slope were determined by drawing pH versus Potential plot (Figure-6b) in this titration.

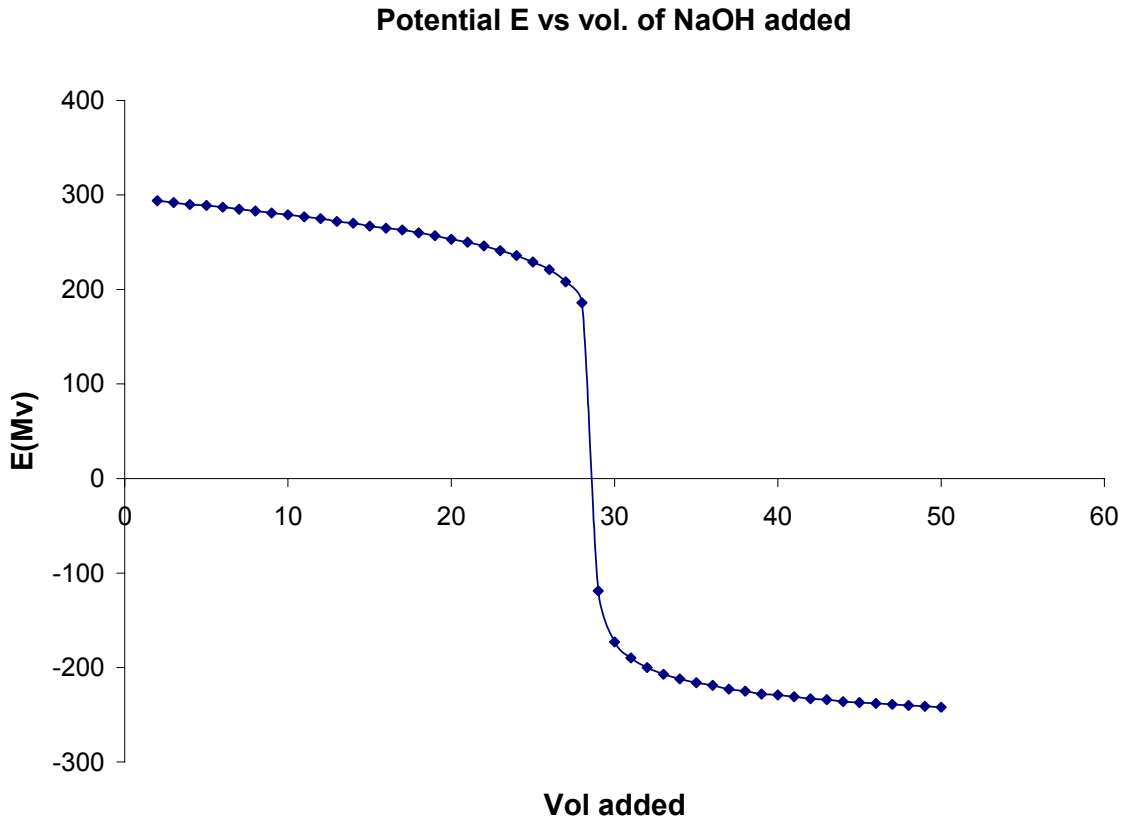

Figure 6(a). Typical titration curve of potential, *E*, versus volume added, for calibration of the glass electrode. The midpoint of the inflection at about 28 ml is the end-point of the acid-base titration, and allows for standardization of the base solution. The titration was for 0.01 *M* NaOH into a standard 0.01 *M* HNO_3 solution. The experimental value of the Nernstian slope and E^o for the cell were calculated from the titration as shown in Figure 8(b).

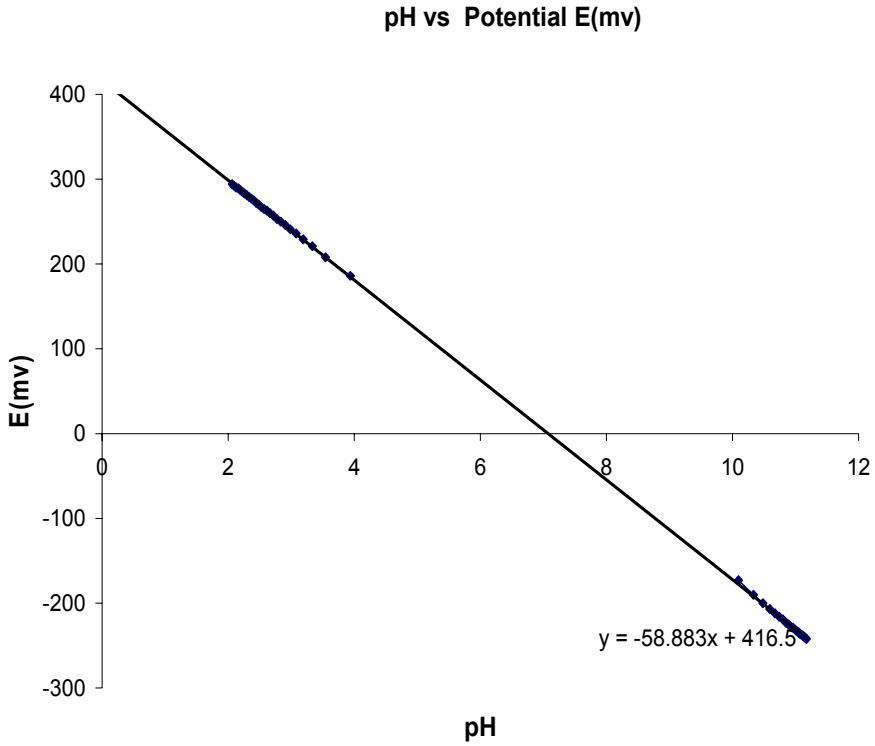

Figure-6(b). Acid-base titration for calibration of the glass electrode. The slope of the plot gives the calculated Nernstian slope of 58.88 mV/decade in this example, and an E^{o} value for the cell of 416.5 mV.

An MS-DOS program (SPECIES-3) written in QBASIC (Hancock, 1985) was used to predict speciation behavior for both the In(III)-1,10 phenanthroline and the Ni(II)-terpyridine complexes as a function of pH. The input data for the program were the appropriate stability constants and protonation constants, either experimental values obtained here, or from the NIST database.[25]

Determination of terpyridine pK_a values

Determination of the pK_a values of the terpyridine complexes of Ni(II) and Zn(II) was carried out by voltammetry. Such pK_a values are considered to correspond to the deprotonation of a coordinated water molecule, as in:

$$[Ni(terpy)H_2O]^{2+} \rightarrow [Ni(terpy)OH]^{+} + H^{+} \quad (5)$$

The pK_a values for the Ni-tpy complex were found by voltammetry.[26-27] A plot of peak position versus pH was generated; from this it was possible to calculate both the first and second pK_a of the metal-ligand complex. The first and second protonation constants, pKa_1 and pKa_2, are given by (L = terpyridine).

$$K_{a1} = [ML(OH_2)OH]/[H^{+}][ML(OH)_2] \quad (6)$$

$$K_{a2} = [ML(OH_2)_2]/[H^{+}][ML(OH_2)OH] \quad (7)$$

Determination of log K for In(III) / 1,10-phenanthroline

Log K values for the In(III)/1,10-phen complexes were determined by titrating 25.00 ml of acidified 10^{-3} *M* 1,10-phen solution plus acidified 0.750 mL 10^{-3} *M* $In(NO_3)_3$ solution with 0.10*M* NaOH in a voltammetric cell fitted with a temperature regulator at 25.00 ± 0.05 °C. Purified nitrogen gas was bubbled through the solution to exclude any oxygen or carbon dioxide. Peaks were recorded in the differential pulse (DP) mode of the

instrument and a modulation amplitude of -0.02505 v per second over the potential range of -0.2 to -1.2 was set. When excess of the ligands appeared (after equivalence point), the system showed labile behavior, and a set of potential *E* data was collected. In labile behavior, the potentials move according to expectations from the Nernst equation, as ligand concentrations change. In contrast, in non-labile behavior, separate peaks are observed for different metal species present in the solution, whose relative peak heights change as ligand concentration is varied.

The total ionic strength of the solutions was kept constant at $I = 0.10$ with $NaNO_3$. From the voltammetric data obtained, it was possible to calculate values of log *K* using the appropriate equation:

$$E = E^{o} + (RT/nF) \cdot \ln [M_{free}]/[M_{initial}] \quad (8)$$

where M_{free} is the concentration of non-complexed metal ion in the presence of the ligand, and $M_{initial}$ is the total concentration of metal ion before any complex is formed. The value of E^{o} in this equation is calculated for the case where no ligand has been added, so that $[M_{free}] = [M_{initial}]$. The value of E^{o} is thus calculated from the position of the DPV peak for the non-complexed In^{3+} aquo ion. As discussed below, there is some uncertainty in determining the position of the DPV peak for the free In^{3+} ion, since the latter produces an extremely weak peak, and E^{o} is determined from this single poorly defined point.

The binding constants for the In(III)/1,10-phen system as determined by voltammetry needed to be validated by another method. This was because, as mentioned above, the DPV peak for the In^{3+} aquo ion is extremely weak, and its potential is difficult to measure accurately. It was therefore decided to check the value of K_1 and K_2 by ^{1}H

NMR. A series of solutions with 0.1% DSS, 10% D_2O, 0.1M $NaNO_3$, 0.001M Indium(III), 0.01M 1,10-phen were prepared. pH values for these solutions were adjusted from 0.1 to 5.3 with increments of approximately 0.5 pH units. All proton signals were assigned using the ^1H NMR spectra of 1,10-phen alone. The chemical shifts of the protons on 1,10-phen were monitored to measure the ^1H NMR shift as a function of pH. A plot of pH versus ^1H shift was constructed from the data obtained above for each proton. The pK_a is indicated by midpoints in the regions of shifting of the ^1H signal as a function of pH.

Fluorescence studies

Fluorimetry was carried out for the confirmation of fluorescence of Ni(II)-terpyridine. FURA-2 was complexed with Ni^{2+}, Cd^{2+}, Cu^{2+}, Zn^{2+} and Ca^{2+} to determine the "order of fluorescence" for the metal ions. For all fluorescence experiments, a 0.1 second integration time and two averaged scans were used. The FURA-2 data was recorded at the excitation wavelength of 360 nm and emission wavelength of 510 nm. For terpyridine data, the excitation wavelength was set at 360 nm. All solutions made up for fluorescence experiments were aqueous; and solutions were purged with N_2 gas prior to each fluorescence experiment. The concentration of ligands was kept constant at 10^{-4} *M*.

RESULTS AND DISCUSSION

Study of the Indium (III)/1,10-phenanthroline system.

Complexes of In(III) with nitrogen donor ligands have not been extensively studied. In this work, the fluorescence properties of the In(III)/1,10-phenanthroline system were studied, and it was found that In(III) did appear to cause a slight CHEF effect, whereas the isoelectronic Zn(II) (both d^{10} ions) produces a strong CHEF effect. In order to verify that In(III) actually forms a complex with 1,10-phen, an NMR and voltammetric study of the In(III) /1,10-phen system were performed.

1H NMR spectra for In(III) / 1,10-phenanthroline

The ^{1}H NMR spectrum of 1,10-phen in Figure 7 is consistent with the molecular structure of 1,10-phen, and the spectrum reported. It shows aromatic peaks between 7.6 to 8.9 ppm, which integrate for a total of 8H. A doublet at 8.9 ppm, which integrates for 2H, is assigned to H2 and H9 of 1,10-phen. Another doublet at 8.3 ppm corresponds to H4 and H7. An apparent multiplet consisting of two overlapping triplets is evident at 7.7 ppm, which represent H3 and H8 of 1,10-phen. A singlet at 7.7 ppm integrates to 2H corresponds to H5 and H6.

NMR was used to assess the proton shifts of 0.01 M 1,10-phen in 50% MQ H_2O/D_2O solution as a function of variation in pH values, so that these would not be confused with changes in the spectrum of 1,10-phen on complex formation with In(III). The pH values of the 1,10-phen solutions were 0.5, 1.1, 1.4, 1.9, 3.7 and 5.3. Each solution was made up to 1.0 M ionic strength, using varying ratios of HNO_3, $NaNO_3$ and NaOH. The resulting spectral overlay is shown in Figure 8. Figure 9 depicts a graph of

peak positions versus pH. The NIST Database[25] lists the first and second pK values (pK_1 and pK_2) of 1,10-phen to be 5.1 and 1.8, respectively. The shifts shown in Figure 9 are consistent with a pK_1 of 4.9, but those down below pH 2 are not consistent with a pK_2 of 1.8, but a much lower value. The pK_2 value for 1,10-phen is a single reported value[25] determined by calorimetry, which seems to be an inherently unreliable method at very low pH.

NMR spectra for 1,10-phen complexed with In(III) were recorded as a function of increasing pH. The concentration of In(III) and 1,10-phen was 0.001 M, and the ionic strength of the solutions was made up to be 0.1M with $NaNO_3$ and standardized with NaOH. The solutions were made up with solvent that was 50% MQ H_2O and 50% D_2O, (99.9%) containing DSS incorporated as a calibration standard. The resulting spectra are shown in Figure 10. The 1H spectra show that as the pH is raised, peaks for the free 1,10-phen ligand disappear, and are replaced by new peaks indicating the formation of the complex. This is consistent with a ligand exchange process that is slow on the NMR time-scale. It is interesting to note that at higher pH the peaks for the ^{1}H signal broaden, which suggest that the exchange process is becoming faster. The relative integration of the NMR signals for the free 1,10-phen and In(III)/1,10-phen complex can be used to calculate the fraction of metal ion to which ligand is bound, which is the $\bar{n}$ function.

$\bar{n}$ = integration 1H peak In(III)phen/(integration total 1,10-phen)

In Figure 11, $\bar{n}$ for 1,10-phen is plotted versus pH. The pH at which 50% of the 1,10-phen is complexed ($\bar{n}$ = 0.5) is used to calculate log K_1 for the In(III) / 1,10-phen complex. This is accomplished using the pK_1 value for 1,10-phen of 4.92 at a 0.1 M ionic strength.[25]

Log K_1 = log [ML]/[M][L]

= log(1/[L]) for $\bar{n}$ = 0.5 (where [ML] = [M])

= pK_1 + log [H^+] - log [HL^+] (substituting for [L] from pK_1 = log[HL] – log [L] – log [H^+])

= 4.92 – 1.37 - log (.001/2) (where .001 is the molarity of 1,10-phen)

= 6.85

The formation constant of 6.85 can be compared with a literature value[25] of 5.7 reported at ionic strength 1.0 M. The latter value was obtained[28] in 1.0 *M* Na_2SO_4. Since log K_1 for the formation of the In(III)/SO_4^{2-} complex is 1.80[25], it would be reasonable to expect log K_1 for the 1,10-phen complex to be depressed if measured in 1.0 *M* Na_2SO_4 because the added factor of competition for the In(III) with the SO_4^{2-} would "take away" from the binding ability of the 1,10-phen to bind with In^{3+}.

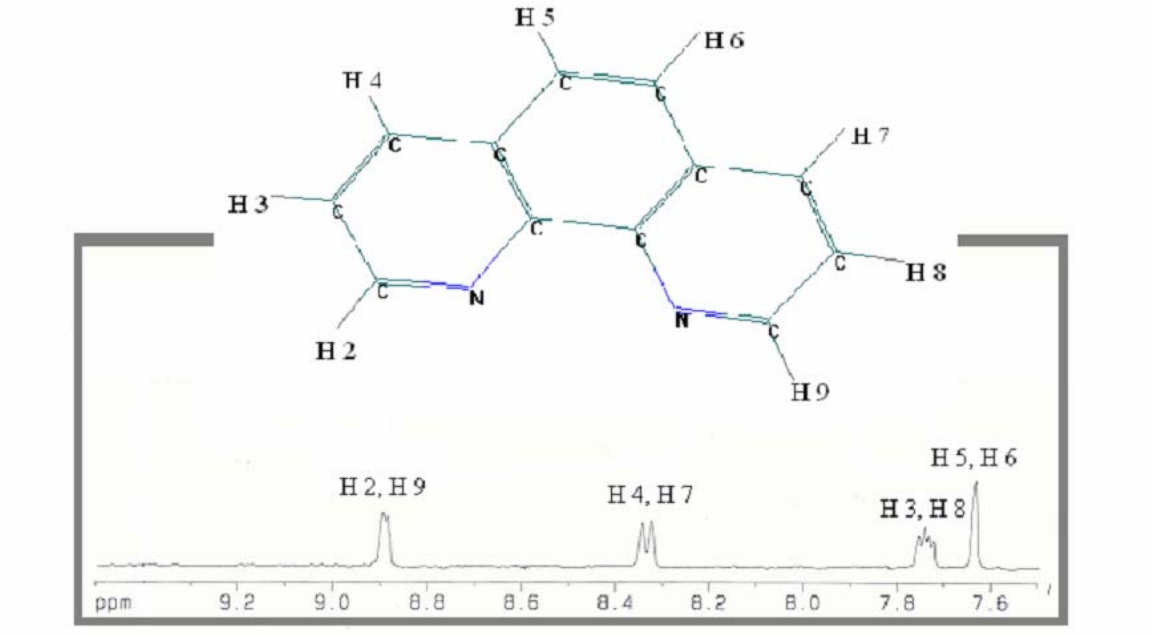

Figure 7. Proton assignments and ^{1}H NMR spectrum for 0.01 M 1,10 phenanthroline in deuterated chloroform.

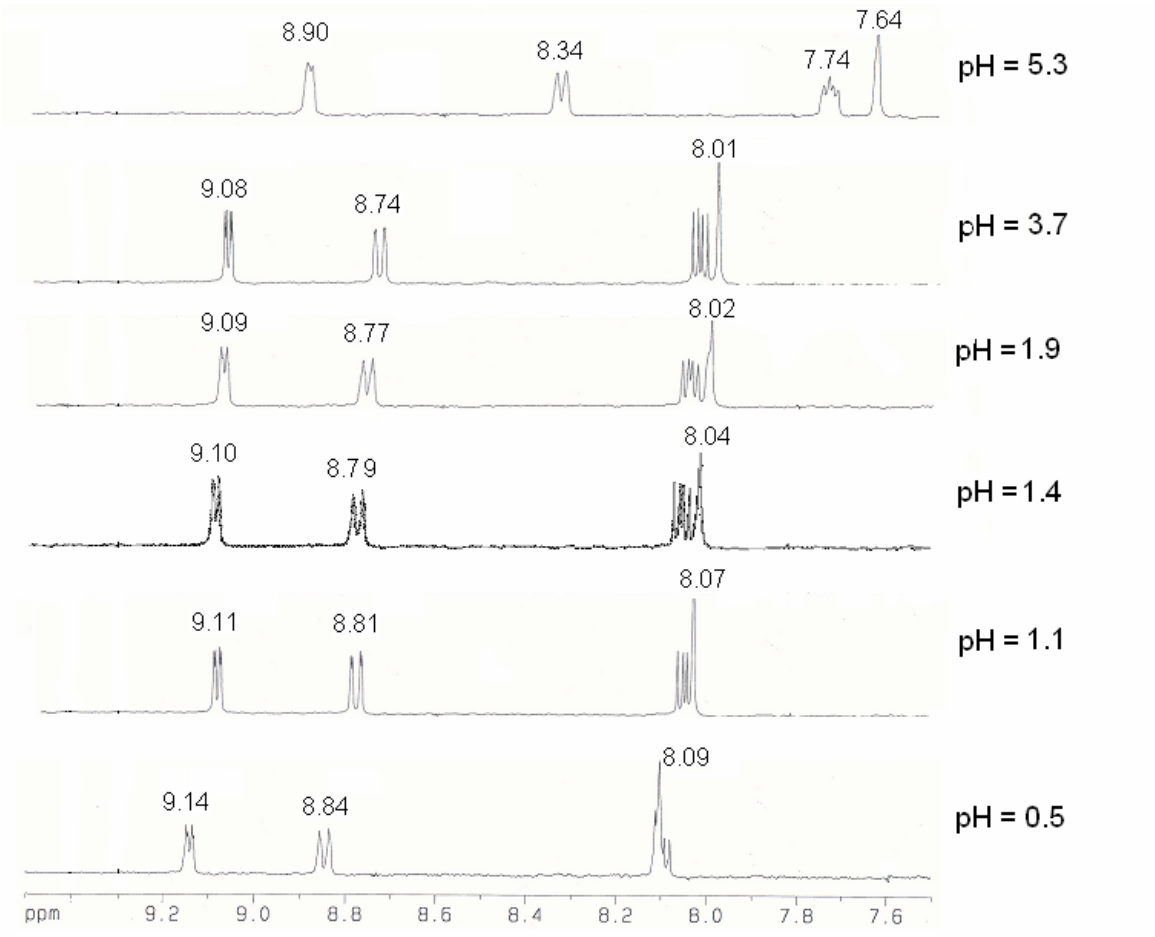

Figure 8. Overlay 1H NMR spectra for 0.001M 1,10-phen aqueous solutions with increasing pH.

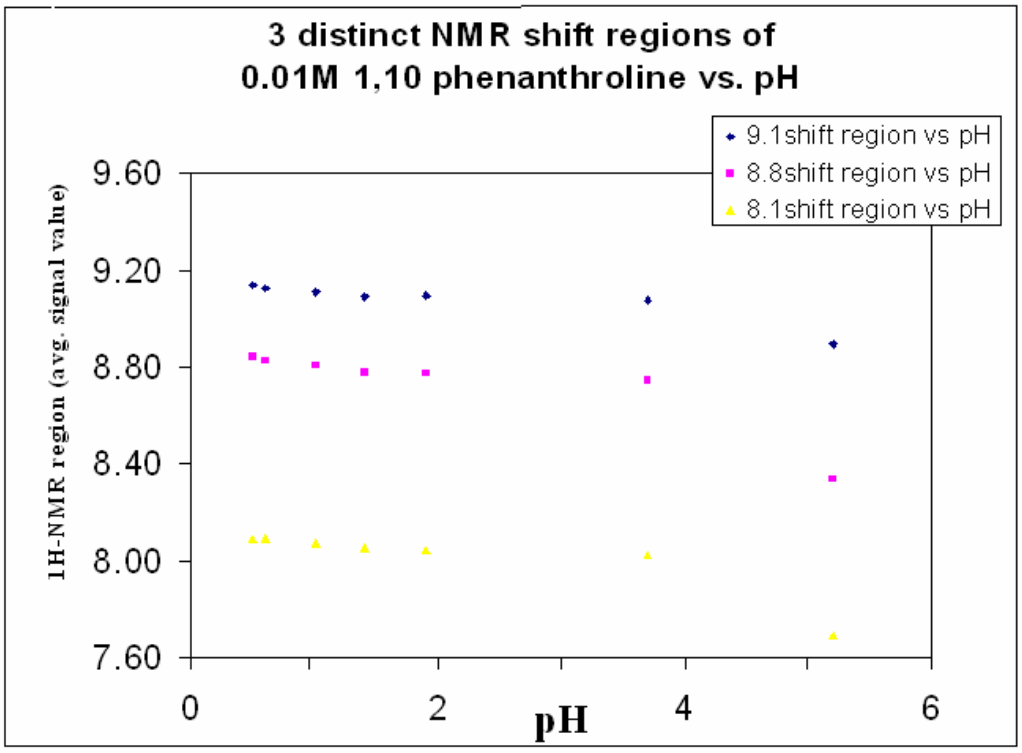

Figure 9. Shift regions of 0.01 M 1,10-phen as a function of pH. The inflections of the signals indicate the pK values for 1,10-phen. The first and second literature values for these are reported as 1.8 and 4.9. The shifts in the pH 3 to 6 range are consistent with a pK_1 of 4.9, but those below pH 2 are not consistent with a pK_2 of 1.8, but a much lower value (<0).

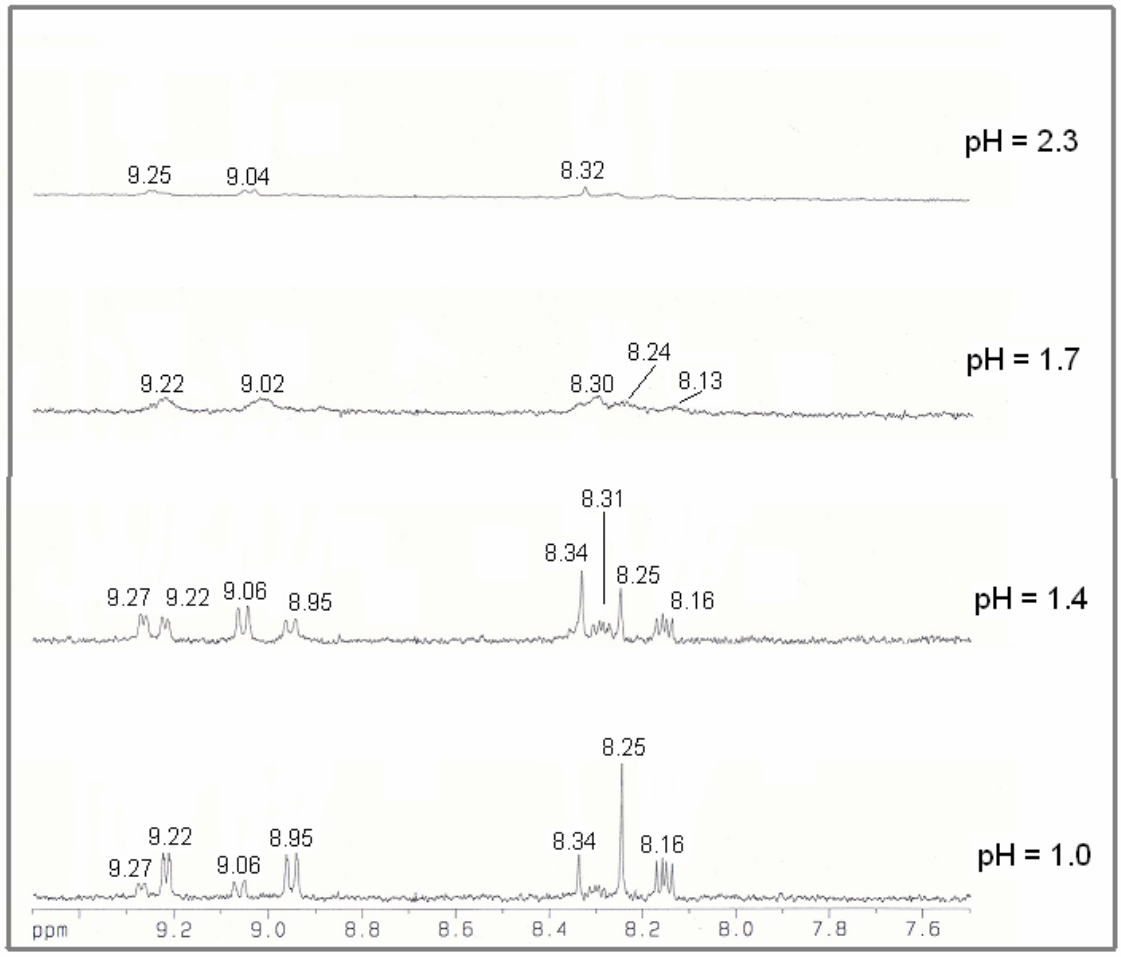

Figure 10. ^{1}H NMR spectra of 0.001 M In(III) / phenanthroline as a function of pH. The peaks as 8.16, 8.25, 8.95, and 9.22 ppm are those of the protonated ligand LH^{+}, while those at 8.34, 9.06, and 9.27 ppm are those of the complex In(III)L (L = 1,10-phen).

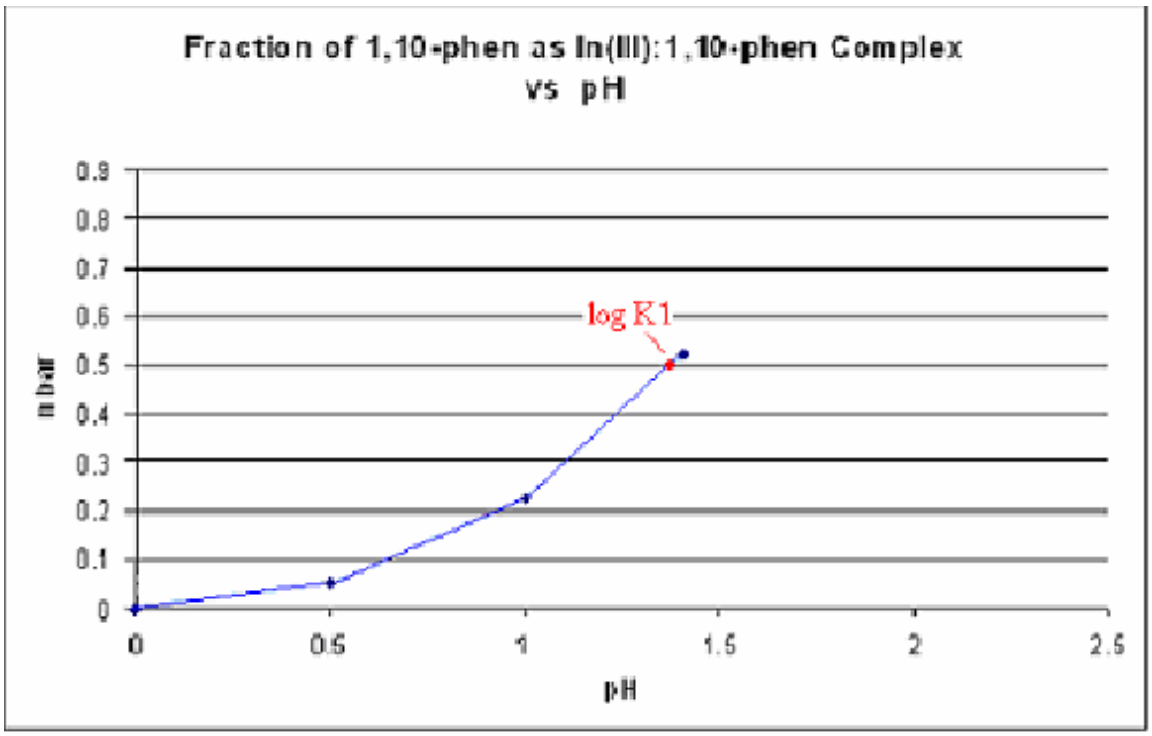

Figure 11. Plot of $\bar{n}$ (n bar) versus pH for In(III)/1,10-phen. Log K_1 for the ML complex (50% complex formation) can be calculated from where $\bar{n} = 0.5$ at a pH of 1.37, indicated as 'log K_1', as discussed in the text.

The experimentally determined log K values for the In(III)/1,10-phen complexes were entered into the QBASIC program SPECIES (Hancock 1985) along with pK values for 1,10-phen and binding constants for Indium(III) hydroxide formation. A graph of speciation in aqueous solution was constructed as a function of increasing pH and is depicted in Figure 12.

Voltammetry of the In(III) / 1,10-phenanthroline complex

Differential pulse voltammetry was performed for the In(III) / phen aqueous solutions (see Experimental for details and conditions). The pH was increased and recorded prior to each voltammetric sweep via small additions of standardized 0.10M NaOH solution. Voltammetric peak positions were assigned by comparing the voltammograms of 1,10-phen alone versus In(III) / 1,10-phen. This comparison is shown in Figure 13. The values of log K_1, log β_2, and log β_3 were calculated from the potentials for the In^{3+} peak, which shifted to more negative potentials as the pH was raised. Three distinct zones (Fig. 14) with differing slopes were considered in equation 8:

$$E_{(obs)} = E_{(init)} - RT/nF \ln [In^{3+}] \qquad [8]$$

where $E_{(obs)}$ is the observed potential for the In^{3+} voltammetric peak in the complex, and $E_{(init)}$ is the potential for the In^{3+} peak in the absence of the ligand. Application of equation 8 gives the concentration $[In^{3+}]$ for each titration point. The calculated value of $[In^{3+}]$ allows for calculation of $\bar{n}$ for each data point from:

$$\bar{n} = In_{(total)} - [In^{3+}] \qquad [9]$$

The values of log K_1, log β_2, and log β_3 were calculated as shown in Table 4 using the Excel program for all calculations and data handling. It is seen that the calculated value of log K1 in Table 4 is 6.65. This is somewhat lower than the value of 6.85 obtained from the NMR experiments described above. This no doubt reflects the difficulty of determining $E_{(init)}$ in equation 7, which is the position of the peak for In^{3+} in the absence of the ligand. The latter peak is extremely weak in the absence of added 1,10-phen, which makes determination of its position difficult. Simply changing *E*(init) from the value of -476 mV used in Table 4 to a value of -473 mV changes the calculated value of log K_1 obtained from the potentials in Table 4 to 4.81, in much better agreement with the NMR value of 4.86. Because of the uncertainty in determining $E_{(init)}$ for In^{3+}, the value of $E_{(init)}$ is here taken to be -473 mV, This gives calculated values for log K_n for the In(III)/1,10-phen system (Ionic strength = 0.1 ($NaNO_3$), T = 25.0 ±0.1 ºC), as shown in Table 5. The much lower literature log β values than those reported here probably reflects, as mentioned above, the fact that the literature values were determined in 1.0 M SO_4^{2-}, which complexes In(III) quite strongly. The work reported here illustrates the unprecedented use of voltammetry for the determination of formation constants with In(III), with the unexpected labile behavior of the In(III)/1,10-phen system. Of particular importance is that the In(III)/1,10-phen complexes show strong peaks in the voltammograms obtained, unlike the In^{3+} aquo ion, which gives a barely detectable peak. Also of considerable interest is the use of 1H NMR to determine log K_1 for the In(III)/1,10-phen complex, as a means of overcoming the difficulty of accurately assigning the In^{3+}(aq) peak in the voltammetric study, in which the peak for the In^{3+} ion is extremely weak. A difference in the series of log K_n values reported here for the

In(III)/1,10-phen system, compared to the literature values[25,28] is that there is a rapid fall-off in the literature values as n increases along the series log K_1, log K_2, log K_3 (Table 5(a)). In contrast, the results for the log K_n values found here fall off only very slowly. The latter results seem very reasonable, as seen in Table 5(b), where literature values of log K_n for Co(II), Ni(II) and Zn(II) are compared with those obtained here for In(III). It is seen that for all these metal ions log K_n decreases only very slowly as n increases, suggesting that the result obtained here for the log K_n values for the In(III)/1,10-phen system are typical of 1,10-phen complexes, and therefore very reasonable.

The utility of NMR in studies in aqueous solution is further illustrated by the study of the protonation of 1,10-phen reported here, which casts serious doubt on the reported[25] pK_2 for this ligand. The lack of a shift in the 1H NMR spectrum of 1,10-phen until a pH of less than 1.0 suggests that the reported value of pK_2 = 1.8 is not correct. This result might have been expected in that the amount of electrostatic repulsion between two protons bound in the close proximity provided by the N-donors of 1,10-phen would be very high, and in retrospect, protonation constants for 1,10-phen of 4.92 and 1.8 seem rather close together (pK_1 – pK_2 = 3.12) when compared to a diamine such as ethylenediamine (en). Here the pK_1 is 9.92 while pK_2 is 7.11, giving pK_1 – pK_2 = 2.81. En has the possibility of free rotation about its C-C bond, so that the two N-donors should be able to rotate away from each other. It seem improbable that 1,10-phen, where the two protons would be forced to remain in close proximity, would have pK_1 – pK_2 differing by so small an amount from that observed for en.

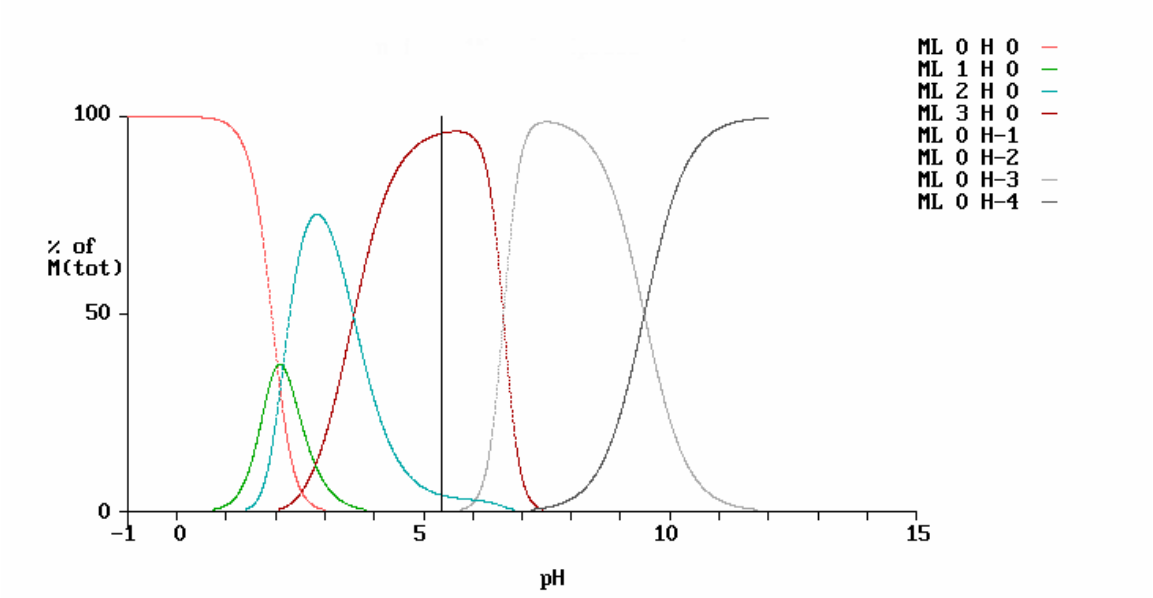

Figure 12. QBASIC speciation diagram of In(III)-phenanthroline as a result of increasing pH. Note the initial free metal (ML 0 H 0), formation of the ML complex (ML 1 H 0) beginning at pH 2.1, and the ML_2 complex (ML 2 H 0) forming at pH 3.1. Note also the solid line at pH 5.4 that indicates the onset of precipitate formation $In^{3+}(aq) + 3OH^{-}(aq) \rightarrow In(OH)_3(s)$.

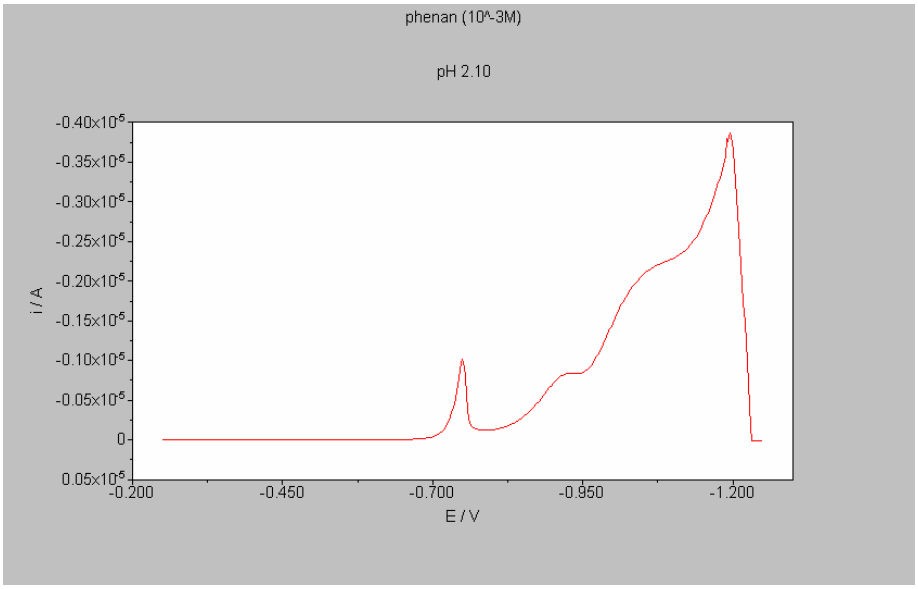

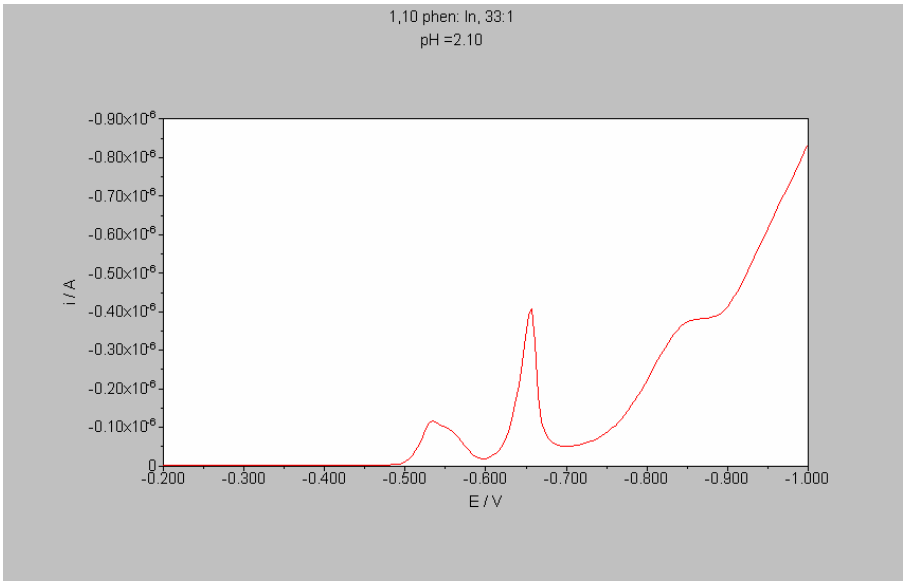

Figure 13. Voltammograms of 1,10-phenanthroline alone (top) and In(III) / phen (bottom), with the same pH of 2.1. Note the complex peak at -0.530 V, which is assigned as the In(III) / phen peak. This peak moves according to a modified form of the Lingane equation, allowing calculation of log K_n values for the system.

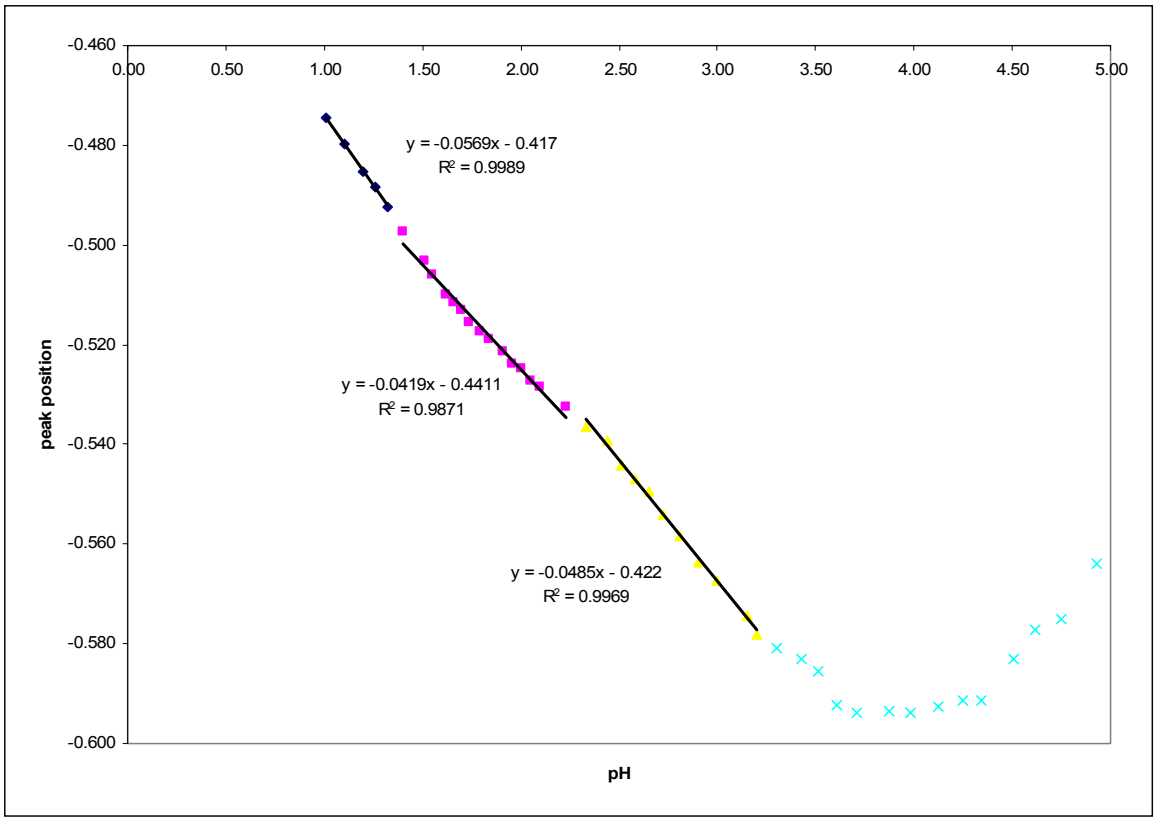

Figure 14. Voltammetric peak position versus pH for the titration of the In(III) / phen with 0.01 M NaOH. The regions of formation of In(III)L (black), In(III)L_2 (pink), and In(III)L_3 (yellow) are indicated by different colors (L = 1.10-phen).

Table 4. Voltammetric data from experiment with 50.00 mL In(III) / phen in 0.1 *M* $NaNO_3$, increasing pH with std. 0.01 *M* NaOH prior to each data point.

pH	peak pos	peak height	vol NaOH added	[In3+]	In(total)	phen total	[Inphen]	[phen]	[H+]	K	log K1	nbar
2.51	-0.581	-8.96E-09	15.500	6.56E-06	7.63E-06	7.63E-05	1.07E-06	2.46E-07	3.07E-03	6.64E+05	5.822	0.140
2.54	-0.579	-1.28E-08	16.000	7.97E-06	7.58E-06	7.58E-05	-3.95E-07	2.69E-07	2.87E-03	-1.84E+05	#NUM!	-0.052
2.57	-0.581	-1.37E-08	16.500	6.11E-06	7.52E-06	7.52E-05	1.41E-06	2.79E-07	2.70E-03	8.26E+05	5.917	0.187
2.59	-0.585	-1.34E-08	17.000	3.72E-06	7.46E-06	7.46E-05	3.75E-06	2.87E-07	2.55E-03	3.51E+06	6.545	0.502
2.63	-0.583	-1.62E-08	17.500	4.53E-06	7.41E-06	7.41E-05	2.88E-06	3.15E-07	2.36E-03	2.01E+06	6.304	0.388
2.66	-0.585	-1.77E-08	18.000	3.49E-06	7.35E-06	7.35E-05	3.87E-06	3.34E-07	2.19E-03	3.32E+06	6.521	0.526
2.69	-0.585	-1.69E-09	18.500	3.40E-06	7.30E-06	7.30E-05	3.90E-06	3.58E-07	2.05E-03	3.20E+06	6.505	0.534
2.73	-0.585	-1.76E-08	19.000	3.32E-06	7.25E-06	7.25E-05	3.93E-06	3.89E-07	1.88E-03	3.04E+06	6.483	0.542
2.76	-0.587	-2.06E-08	19.500	2.58E-06	7.19E-06	7.19E-05	4.62E-06	4.20E-07	1.73E-03	4.27E+06	6.630	0.642
2.81	-0.589	-2.19E-08	20.000	2.00E-06	7.14E-06	7.14E-05	5.14E-06	4.67E-07	1.55E-03	5.51E+06	6.741	0.720
2.85	-0.589	-2.12E-08	20.500	1.98E-06	7.09E-06	7.09E-05	5.11E-06	5.15E-07	1.40E-03	5.00E+06	6.699	0.720
2.90	-0.593	-2.38E-08	21.000	1.24E-06	7.04E-06	7.04E-05	5.80E-06	5.71E-07	1.25E-03	8.20E+06	6.914	0.824
2.96	-0.593	-3.10E-08	21.500	1.25E-06	6.99E-06	6.99E-05	5.74E-06	6.52E-07	1.10E-03	7.05E+06	6.848	0.821
3.03	-0.595	-4.08E-08	22.000	9.24E-07	6.94E-06	6.94E-05	6.02E-06	7.59E-07	9.38E-04	8.59E+06	6.934	0.867
3.11	-0.599	-4.42E-08	22.500	5.79E-07	6.90E-06	6.90E-05	6.32E-06	9.01E-07	7.85E-04	1.21E+07	7.083	0.916
3.20	-0.603	-5.88E-08	23.000	3.63E-07	6.85E-06	6.85E-05	6.49E-06	1.10E-06	6.38E-04	1.62E+07	7.210	0.947
3.31	-0.607	-8.42E-08	23.500	2.28E-07	6.80E-06	6.80E-05	6.58E-06	1.42E-06	4.93E-04	2.04E+07	7.309	0.967
3.46	-0.615	-1.79E-07	24.000	8.94E-08	6.76E-06	6.76E-05	6.67E-06	2.01E-06	3.44E-04	3.71E+07	7.569	0.987
3.70	-0.633	-3.42E-07	24.500	1.09E-08	6.71E-06	6.71E-05	6.70E-06	3.36E-06	2.01E-04	1.82E+08	8.261	0.998
3.88	-0.645	-4.01E-07	25.000	2.69E-09	6.67E-06	6.67E-05	6.66E-06	4.98E-06	1.32E-04	4.97E+08	8.697	1.000

mean: 6.6477
stdev: 0.1992

Table 5(a). Formation constants for the In(III)/1,10-phenanthroliine system determined here by NMR and voltammetry (Ionic strength 0.1, T = 25 ^{o}C), together with literature values for comparison.[25]

						Literature value of log β [25]
log K_1	=	6.81				5.7
log K_2	=	6.44	log β_2	=	13.25	10.0
log K_3	=	6.20	log β_3	=	19.45	14.0

Table 5(b). Comparison of log K_n values for 1,10-phenanthroline complexes of a variety of metal ions.[25]

Metal ion	log K_1	log K_2	log K_3
In(III)	6.8	6.4	6.2
Co(II)	7.1	6.6	6.0
Ni(II)	8.7	8.1	7.6
Zn(II)	6.4	5.7	5.0

The Crystal Structure of $[Ni(terpy)_2][Ni(CN)_4]$ and $[Cd(neocuproine)(NCS)_2]_2$

In the fluorescence study of the terpy complex of Ni(II), results were found that suggested that the complex being formed in solution was not the expected $[Ni(terpy)CN]^+$, but that what was being observed was disproportionation according to the following equilibrium, which appeared to lie far to the right:

$$4[Ni(terpy)CN]^+ \leftrightarrows [Ni(terpy)_2]^{2+} + 2\,[Ni(terpy)(H_2O)_3]^{2+} + [Ni(CN)_4]^{2-} \quad [9]$$

In order to test this hypothesis, crystals were grown from a 1:1:1 Ni(II)/terpy/CN^- solution, and the structure of the resulting complex was determined to see whether the $[Ni(CN)_4]^{2-}$ complex was being formed by disproportionation as suggested by reaction [9] above. The structure of the synthesized complex is reported below.

Data obtained from the crystallographic determination of $[Ni(terpy)_2][Ni(CN)_4]$ is reported in Figures 15 and 16, and Tables 6-9. The crystallographic data show that the Ni(II) exists as a six coordinate *bis*-terpyridine complex, with a square-planar four coordinate $Ni(CN)_4^{2-}$ anion as the counter ion. The disproportionation in reaction [9] explains the increase in fluorescence as a result of adding the NaCN solution to the Ni (II) / terpyridine solution, since there appears to be a further slow disproportionation according to:

$$[Ni(terpy)_2]^{2+} + H^+ \leftrightarrows [Ni(terpy)(H_2O)_3]^{2+} + terpyH^+ \text{ (fluorescent cplx.)} \quad [10]$$

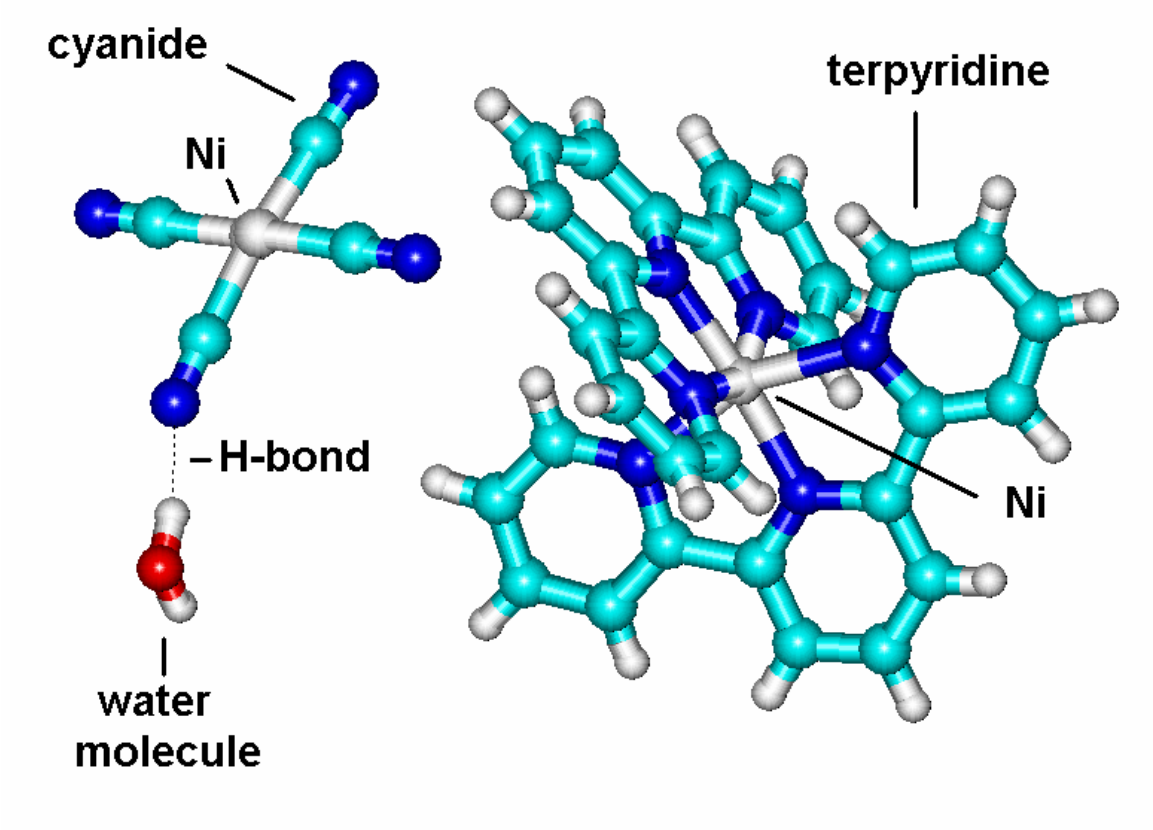

Figure 15. Molecular drawing of $[Ni(terpy)_2][Ni(CN)_4]$. At left is the $[Ni(CN)_4]^{2-}$ ion, with an H-bonded water molecule, and at right the $[Ni(terpy)_2]^{2+}$ cation. Drawing made using the program HyperChem.[24]

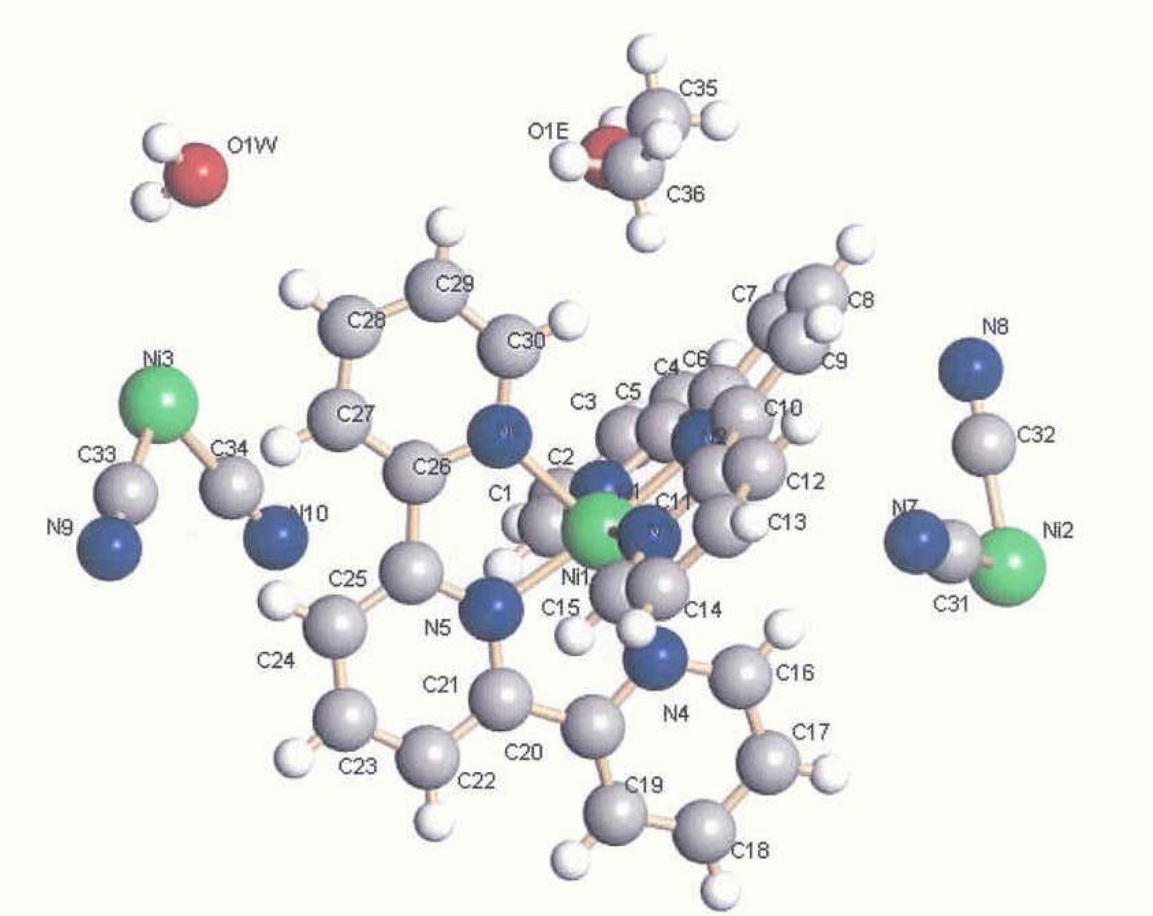

Figure 16. The structure of $[Ni(terpy)_2][Ni(CN)_4]$, showing the numbering scheme.

Table 6. Crystal data and structure refinement for $[Ni(terpy)_2][Ni(CN)_4]$

Empirical formula	C18 H15 N5 Ni O
Formula weight	376.06 g/mol
Temperature	110(2) K
Wavelength	0.71073 Å
Crystal system	Triclinic
Space group	P-1
Unit cell dimensions	a = 8.644(3) Å b = 9.840(3) Å c = 20.162(6) Å α = 97.355(5)°. β = 97.100(5)°. γ = 98.606(5)°.
Volume	1663.8(9) Å3
Z	4
Density (calculated)	1.501 Mg/m3
Absorption coefficient	1.182 mm-1
F(000)	776
Crystal size	0.40 x 0.10 x 0.10 mm3
Theta range for data collection	1.03 to 25.00°.
Index ranges	-10<=h<=10, -11<=k<=11, -23<=l<=23
Reflections collected	15699
Independent reflections	5836 [R(int) = 0.0310]
Completeness to theta =	25.00° 99.6 %
Max. and min. transmission	0.8909 and 0.6492
Refinement method	Full-matrix least-squares on F2
Data / restraints / parameters	5836 / 0 / 454
Goodness-of-fit on F2	1.023
Final R indices [I>2sigma(I)]	R1 = 0.0319, wR2 = 0.0798
R indices (all data)	R1 = 0.0375, wR2 = 0.0900

Table 7. Atomic coordinates (x 10^4) and equivalent isotropic displacement parameters ($Å^2$ x 10^3) for $[Ni(terpy)_2][Ni(CN)_4]$.

	x	y	z	U(eq)
Ni(1)	454(1)	2878(1)	7361(1)	14(1)
Ni(2)	0	10000	10000	21(1)
Ni(3)	5000	5000	5000	20(1)
O(1E)	-5783(3)	7712(3)	8688(1)	39(1)
O(1W)	4646(3)	-405(2)	5854(1)	38(1)
N(1)	2617(3)	2167(2)	7618(1)	17(1)
N(2)	1002(3)	3647(2)	8339(1)	16(1)
N(3)	-1521(3)	3808(2)	7537(1)	16(1)
N(4	-811(2)	861(2)	7299(1)	16(1)
N(5	-5(2)	2289(2)	6366(1)	16(1)
N(6)	1538(2)	4643(2)	6999(1)	16(1)
N(7)	1597(3)	7871(3)	10654(1)	27(1)
N(8	-2887(3)	7813(3)	9512(1)	32(1)
N(9)	1915(3)	4514(3)	4060(1)	27(1)
N(10)	4239(3)	2140(3)	5386(2)	38(1)
C(1)	3331(3)	1344(3)	7225(1)	20(1)
C(2)	4695(3)	867(3)	7459(2)	23(1)
C(3)	5332(3)	1252(3)	8132(2)	25(1)
C(4)	4613(3)	2116(3)	8543(2)	23(1)
C(5)	3251(3)	2563(3)	8278(1)	18(1)
C(6)	2398(3)	3503(3)	8671(1)	18(1)
C(7)	2946(3)	4238(3)	9309(1)	23(1)
C(8)	2053(3)	5161(3)	9584(1)	25(1)
C(9)	625(3)	5318(3)	9234(1)	22(1)
C(10)	115(3)	4512(3)	8608(1)	17(1)
C(11)	-1384(3)	4532(3)	8165(1)	17(1)
C(12)	-2558(3)	5232(3)	8372(2)	22(1)
C(13)	-3913(3)	5186(3)	7920(2)	24(1)
C(14)	-4064(3)	4447(3)	7280(2)	23(1)
C(15)	-2846(3)	3768(3)	7106(1)	19(1)
C(16)	-1097(3)	170(3)	7812(1)	20(1)
C(17)	-1839(3)	-1199(3)	7716(2)	24(1)
C(18)	-2270(4)	-1888(3)	7064(2)	28(1)
C(19)	-1990(3)	-1182(3)	6525(2)	24(1)
C(20)	-1270(3)	192(3)	6657(1)	18(1)
C(21)	-905(3)	1049(3)	6126(1)	17(1)
C(22)	-1407(3)	676(3)	5438(1)	21(1)

Table 7 (contd.)

	x	y	z	U(eq)
C(23)	-914(3)	1598(3)	5010(1)	23(1)
C(24)	49(3)	2853(3)	5260(1)	20(1)
C(25)	471(3)	3185(3)	5956(1)	16(1)
C(26)	1419(3)	4514(3)	6317(1)	17(1)
C(27)	2118(3)	5551(3)	5994(1)	21(1)
C(28)	2957(3)	6766(3)	6378(2)	24(1)
C(29)	3058(3)	6910(3)	7073(2)	23(1)
C(30)	2331(3)	5835(3)	7363(1)	19(1)
C(31)	987(3)	8684(3)	10407(1)	22(1)
C(32)	-1793(4)	8653(3)	9698(1)	24(1)
C(33)	3109(3)	4691(3)	4403(1)	22(1)
C(34)	4519(3)	3229(3)	5241(2)	26(1)
C(35)	-6516(4)	8662(3)	9078(2)	30(1)
C(36)	-8006(4)	8867(4)	8666(2)	33(1)

U(eq) is defined as one third of the trace of orthogonalized Uij tensor.

Table 8. Bond lengths [Å] for $[Ni(terpy)_2][Ni(CN)_4]$.

Ni(1)-N(5)	1.990(2)	C(27)-C(28)	1.385(4)
Ni(1)-N(2)	1.990(2)	C(28)-C(29)	1.381(4)
Ni(1)-N(4)	2.099(2)	C(29)-C(30)	1.380(4)
Ni(1)-N(3)	2.101(2)	C(35)-C(36)	1.499(4)
Ni(1)-N(6)	2.106(2)	Ni(1)-N(1)	2.121(2)
Ni(2)-C(32)#1	1.865(3)	Ni(2)-C(32)	1.865(3)
Ni(2)-C(31)	1.873(3)	Ni(2)-C(31)#1	1.873(3)
Ni(3)-C(33)#2	1.867(3)	Ni(3)-C(33)	1.867(3)
Ni(3)-C(34)	1.869(3)	Ni(3)-C(34)#2	1.869(3)
O(1E) -C(35)	1.417(4)	N(1)-C(1)	1.332(4)
N(1)-C(5)	1.358(3)	N(2)-C(10)	1.337(3)
N(2)-C(6)	1.342(3)	N(3)-C(15)	1.341(3)
N(3)-C(11)	1.353(3)	N(4)-C(16)	1.337(4)
N(4)-C(20)	1.357(3)	N(5)-C(25)	1.338(3)
N(5)-C(21)	1.342(3)	N(6)-C(30)	1.341(3)
N(6)-C(26)	1.354(3)	N(7)-C(31)	1.153(4)
N(8)-C(32)	1.147(4)	N(9)-C(33)	1.146(4)
N(10)-C(34)	1.146(4)	C(1)-C(2)	1.386(4)
C(2)-C(3)	1.380(4)	C(3)-C(4)	1.379(4)
C(4)-C(5)	1.387(4)	C(5)-C(6)	1.480(4)
C(6)-C(7)	1.382(4)	C(7)-C(8)	1.384(4)
C(8)-C(9)	1.384(4)	C(9)-C(10)	1.385(4)
C(10)-C(11)	1.485(4)	C(11)-C(12)	1.385(4)
C(12)-C(13)	1.383(4)	C(13)-C(14)	1.378(4)
C(14)-C(15)	1.386(4)	C(16)-C(17)	1.381(4)
C(17)-C(18)	1.379(4)	C(18)-C(19)	1.388(4)
C(19)-C(20)	1.379(4)	C(20)-C(21)	1.481(4)
C(21)-C(22)	1.386(4)	C(22)-C(23)	1.386(4)
C(23)-C(24)	1.380(4)	C(24)-C(25)	1.389(4)

Table 9. Bond angles [°] for $[Ni(terpy)_2][Ni(CN)_4]$

N(5)-Ni(1)-N(2)	174.50(9)	N(5)-Ni(1)-N(4)	78.56(9)
N(2)-Ni(1)-N(4)	106.92(9)	N(5)-Ni(1)-N(3)	101.06(9)
N(2)-Ni(1)-N(3)	78.42(9)	N(4)-Ni(1)-N(3)	92.92(9)
N(5)-Ni(1)-N(6)	78.15(9)	N(2)-Ni(1)-N(6)	96.37(9)
N(4)-Ni(1)-N(6)	156.71(9)	N(3)-Ni(1)-N(6)	91.84(9)
N(5)-Ni(1)-N(1)	102.42(9)	N(2)-Ni(1)-N(1)	78.30(9)
N(4)-Ni(1)-N(1)	90.79(9)	N(3)-Ni(1)-N(1)	156.50(9)
N(6)-Ni(1)-N(1)	93.87(8)	C(32)#1-Ni(2)-C(32)	180.00(14)
C(32)#1-Ni(2)-C(31)	90.38(12)	C(32)-Ni(2)-C(31)	89.62(12)
C(32)#1-Ni(2)-C(31)#1	89.62(12)	C(32)-Ni(2)-C(31)#1	90.38(12)
C(31)-Ni(2)-C(31)#1	180.00(15)	C(33)#2-Ni(3)-C(33)	180.000(1)
C(33)#2-Ni(3)-C(34)	89.44(12)	C(33)-Ni(3)-C(34)	90.56(12)
C(33)#2-Ni(3)-C(34)#2	90.56(12)	C(33)-Ni(3)-C(34)#2	89.44(12)
C(34)-Ni(3)-C(34)#2	180.000(1)	C(1)-N(1)-C(5)	118.9(2)
C(1)-N(1)-Ni(1)	127.68(18)	C(5)-N(1)-Ni(1)	113.34(17)
C(10)-N(2)-C(6)	121.4(2)	C(10)-N(2)-Ni(1)	118.36(17)
C(6)-N(2)-Ni(1)	119.02(18)	C(15)-N(3)-C(11)	118.4(2)
C(15)-N(3)-Ni(1)	127.86(19)	C(11)-N(3)-Ni(1)	113.75(17)
C(16)-N(4)-C(20)	118.7(2)	C(16)-N(4)-Ni(1)	127.15(18)
C(20)-N(4)-Ni(1)	113.99(17)	C(25)-N(5)-C(21)	121.9(2)
C(25)-N(5)-Ni(1)	119.15(18)	C(21)-N(5)-Ni(1)	118.68(18)
C(30)-N(6)-C(26)	118.0(2)	C(30)-N(6)-Ni(1)	127.62(18)
C(26)-N(6)-Ni(1)	114.35(17)	N(1)-C(1)-C(2)	122.8(3)
C(3)-C(2)-C(1)	118.5(3)	C(4)-C(3)-C(2)	119.2(3)
C(3)-C(4)-C(5)	119.6(3)	N(1)-C(5)-C(4)	121.0(3)
N(1)-C(5)-C(6)	115.0(2)	C(4)-C(5)-C(6)	124.0(2)
N(2)-C(6)-C(7)	120.5(3)	N(2)-C(6)-C(5)	113.6(2)

Symmetry transformations used to generate equivalent atoms:
#1 -x,-y+2,-z+2 #2 -x+1,-y+1,-z+1

The structure of $[Cd(neocuproine)(SCN)_2]_2$

The phosphorescence properties of $[Cu(neocuproine)_2]^+$ suggested that the steric hindrance provided by the methyl groups on the 2,9 positions of neocuproine might also control the coordination geometry of other metal ions to be strictly tetrahedral as found in $[Cu(neocuproine)_2]^+$. A particular question was whether small secondary ligands such as thiocyanate (SCN^-) might not also provide sufficient rigidity to a complex such as $[Cu(neocuproine)(SCN)_2]^-$ that strong phosphorescence might be observed. The general interest here is whether such complexes might not contain a tetrahedral metal ion, which would promote binding of the SCN^- through S rather than N. Cd(II) is anomalous in that, although it is classified as 'soft' in the HSAB classification (see Table 2c), it is almost never bound to SCN^- through the S, except when the SCN^- is bridging, so that both the Sand N are bound to separate Cd(II) ions. Bonding to S is generally regarded as an indicator of soft behavior. As part of the general investigation of the coordinating properties of neocuproine, the complex $[Cd(neocuproine)(SCN)_2]$ was synthesized, and its structure determined, which is reported below.

The structure of $[Cd(neocuproine)(SCN)_2]_2$ is seen in Figs. 17 and 18, which show that it is a dimer that contains two SCN^- groups bridging between the two Cd(II) ions, as well as two non-bridging thiocyanates that are N-bonded. Each Cd(II) is five-coordinate, so that the possibility that it would be tetrahedral with S-bonded thiocyanate groups was not realized. It seems that the steric constraints provided by a single neocuproine ligand is not sufficient to force four-coordination on Cd(II). The five coordination observed here may be sufficient to favor bonding of the SCN^- through the small N-donor rather than the large S-donor of SCN^-.

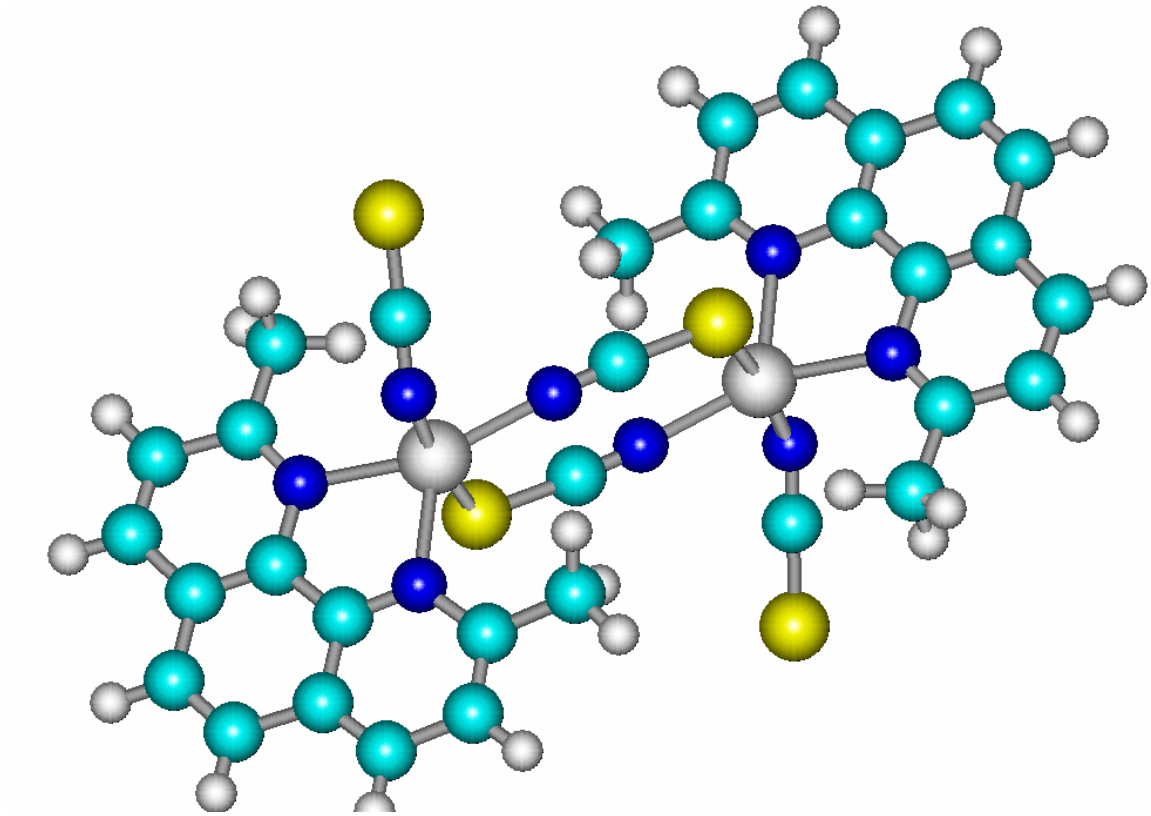

Figure 17. HyperChem[24] drawing of the structure of $[Cd(neocuproine)(NCS)_2]_2$

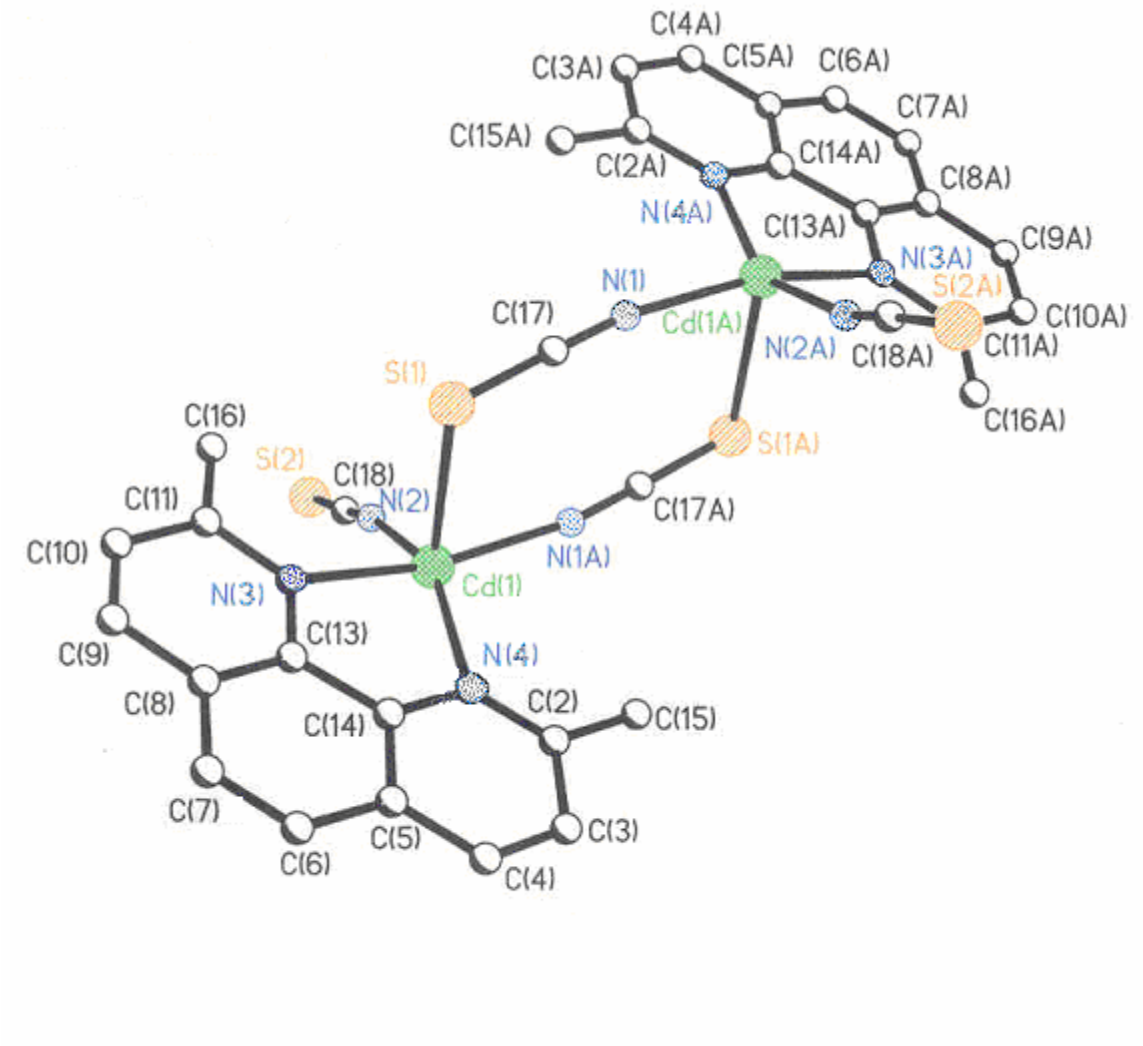

Figure 18. The crystal structure of [Cd(neocuproine)$(NCS)_2]_2$.

Table 10. Crystal data and structure refinement for $[Cd(neocuproine)(NCS)_2]_2$

Empirical formula	C36 H24 Cd2 N4 S4
Formula weight	865.63
Temperature	163(2) K
Wavelength	0.71073 A
Crystal system, space group	Triclinic, P-1
Unit cell dimensions	a = 8.7810(18) Å b = 9.3590(19) Å c = 10.608(2) Å α = 90.34(3)°. β = 94.60(3)°. γ = 111.44(3)°.
Volume	808.3(3) $Å^3$
Z, Calculated density	1.778 Mg/m^3
Absorption coefficient	1.608 mm^{-1}
F(000)	428
Crystal size	0.19 x 0.12 x 0.10 mm
Theta range for data collection	1.93 to 25.00 deg.
Limiting indices	-10<=h<=10, -11<=k<=11, -12<=l<=12
Reflections collected / unique	10429 / 2819 [R(int) = 0.0981]
Completeness to theta = 25.00	99.1 %
Absorption correction	None
Max. and min. transmission	0.8558 and 0.7498
Refinement method	Full-matrix least-squares on F^2
Data / restraints / parameters	2819 / 0 / 218
Goodness-of-fit on F^2	1.116
Final R indices [I>2sigma(I)]	R1 = 0.1617, wR2 = 0.4366
R indices (all data)	R1 = 0.1709, wR2 = 0.4420
Largest diff. peak and hole	8.030 and -2.123 e.A^-3

Table 11. Atomic coordinates (x 10^4) and equivalent isotropic displacement parameters ($Å^2$ x 10^3) for $[Cd(neocuproine)(NCS)_2]_2$

	x	y	z	U(eq)
Cd(1)	4134(2)	3127(2)	7379(2)	26(1)
S(1)	5567(9)	2395(8)	5306(6)	33(2)
N(1)	5960(30)	4900(30)	3700(20)	32(5)
N(4)	1550(20)	1140(20)	6870(19)	13(4)
C(2)	190(30)	1330(40)	6400(20)	34(6)
C(3)	-1300(40)	40(30)	6240(30)	39(7)
C(4)	-1380(30)	-1340(40)	6650(30)	41(7)
C(5)	30(30)	-1560(30)	7150(30)	33(6)
C(6)	50(30)	-3050(30)	7500(30)	35(6)
C(7)	1420(40)	-3180(30)	7970(30)	45(8)
C(8)	2960(30)	-1900(30)	8120(20)	31(6)
C(9)	4440(40)	-2020(40)	8610(30)	42(7)
C(10)	5820(40)	-800(30)	8740(20)	33(6)
C(11)	5890(40)	660(40)	8390(30)	45(8)
N(3)	4450(30)	830(20)	7943(19)	17(4)
C(13)	3010(30)	-450(30)	7800(20)	27(5)
C(14)	1510(30)	-250(30)	7230(20)	25(5)
C(15)	250(30)	2870(30)	6000(20)	34(6)
C(16)	7350(30)	2070(40)	8510(30)	37(7)
C(17)	5820(30)	3850(30)	4360(30)	31(6)
C(18)	6820(30)	5670(30)	9510(20)	28(6)
N(2)	6080(30)	4840(30)	8710(20)	33(5)
S(2)	7971(7)	6964(8)	10637(6)	30(2)

U(eq) is defined as one third of the trace of the orthogonalized Uij tensor.

Table 12.. Hydrogen coordinates (x 10^4) and isotropic displacement parameters ($Å^2$ x 10^3) for [Cd(neocuproine)$(NCS)_2]_2$

	x	y	z	U(eq)
H(3)	-2266	151	5836	100(200)
H(4)	-2424	-2177	6596	0(50)
H(6)	-937	-3949	7384	20(60)
H(7)	1395	-4176	8220	30(70)
H(9)	4456	-3003	8843	40(80)
H(10)	6812	-917	9091	40(80)
H(15A)	522	3554	6727	80(70)
H(15B)	-804	2779	5601	80(70)
H(15C)	1066	3257	5410	80(70)
H(16A)	7232	2778	7897	160(150)
H(16B)	8304	1836	8377	160(150)
H(16C)	7479	2527	9347	160(150)

Table 13. Bond lengths [Å] for $[Cd(neocuproine)(NCS)_2]_2$

Cd(1)-N(1)#1	2.20(2)	Cd(1)-N(2)	2.25(2)
Cd(1)- N(3)	2.34(2)	Cd(1)-N(4)	2.37(19)
Cd(1)-S(1)	2.82(7)	Cd(1)-S(2)#2	2.89(7)
S(1)-C(17)	1.65(3)	N(1)-C(17)	1.19(4)
N(1)-Cd(1)#1	2.20(2)	N(4)-C(2)	1.33(3)
C(1)-C(14)	1.34(3)	C(2)-C(3)	1.42(4)
C(2)-C(15)	1.49(4)	C(3)-C(4)	1.34(4)
C(4)-C(5)	1.39(4)	C(5)-C(14)	1.42(4)
C(5)-C(6)	1.46(4)	C(6)-C(7)	1.31(4)
C(7)-C(8)	1.44(4)	C(8)-C(13)	1.39(4)
C(8)-C(9)	1.41(4)	C(9)-C(10)	1.33(4)
C(10)-C(11)	1.40(4)	C(11)-N(3)	1.38(4)
C(11)-C(16)	1.46(4)	N(3)- C(13)	1.38(3)
C(13)-C(14)	1.48(4)	C(18)-N(2)	1.14(3)
C(18)-S(2)	1.67(3)	S(2)-Cd(1)#2	2.89(7)

Table 14. Bond angles [deg] for[Cd(neocuproine)$(NCS)_2]_2$

N(1)#1-Cd(1)-N(2)	86.9(9)	C(7)-C(6)-C(5)	120.0(3)
N(1)#1-Cd(1)-N(3)	162.7(8)	C(6)-C(7)-C(8)	123.0(3)
N(2)-Cd(1)-N(3)	101.5(8)	C(13)-C(8)-C(9)	117.0(3)
N(1)#1-Cd(1)-N(4)	105.3(8)	C(13)-C(8)-C(7)	119.0(2)
N(2)-Cd(1)-N(4)	153.8(8)	C(9)-C(8)-C(7)	124.0(3)
C(4)-C(3)-C(2)	121.0(3)	C(10)-C(9)-C(8)	121.0(3)
C(12)-Cd(1)-N(4)	73.5(7)	C(9)-C(10)-C(11)	122.0(3)
N(1)#1-Cd(1)-S(1)	86.3(6)	N(3)-C(11)-C(10)	118.0(3)
N(2)-Cd(1)-S(1)	110.0(5)	N(3)-C(11)-C(16)	116.0(3)
N(3)-Cd(1)-S(1)	76.7(5)	C(10)-C(11)-C(16)	126.0(3)
N(4)-Cd(1)-S(1)	94.1(5)	C(11)-N(3)-C(13)	119.0(2)
N(1)#1-Cd(1)-S(2)#2	102.3(6)	C(11)-N(3)-Cd(1)	126.0(2)
N(2)-Cd(1)-S(2)#2	83.8(5)	C(13)-N(3)-Cd(1)	114.2(16)
N(3)-Cd(1)-S(2)#2	93.7(5)	N(3)-C(13)-C(8)	122.0(2)
N(4)-Cd(1)-S(2)#2	71.1(5)	N(3)-C(13)-C(14)	118.0(2)
S(1)-Cd(1)-S(2)#2	164.4(2)	C(8)-C(13)-C(14)	120.0(2)
C(17)-S(1)-Cd(1)	104.1(9)	N(4)-C(14)-C(5)	122.0(2)
C(17)-N(1)-Cd(1)#1	170.6(19)	N(4)-C(14)-C(13)	121.0(2)
C(2)-N(4)-C(14)	120.0(2)	C(5)-C(14)-C(13)	117.0(2)
C(2)-N(4)-Cd(1)	125.9(18)	N(1)-C(17)-S(1)	178.0(2)
C(14)-N(4)-Cd(1)	113.5(15)	N(2)-C(18)-S(2)	177.0(2)
N(4)-C(2)-C(3)	119.0(3)	C(18)-N(2)-Cd(1)	167.0(2)
N(4)-C(2)-C(15)	120.0(2)	C(18)-S(2)-Cd(1)#2	106.6(9)
C(3)-C(2)-C(15)	121.0(3)	C(14)-C(5)-C(6)	120.0(2)
C(3)-C(4)-C(5)	121.0(3)	C(4)-C(5)-C(6)	123.0(2)
C(4)-C(5)-C(14)	116.0(3)		

Symmetry transformations used to generate equivalent atoms:
#1 -x+1,-y+1,-z+1 #2 -x+1,-y+1,-z+2

CHEF Effect of FURA-2 with Zn^{2+}, Ca^{2+}, Cu^{2+}, Ni^{2+}, and Bi^{3+}

FURA-2 has been used primarily as a fluorescent marker to quantify intercellular Ca(II) levels.[19] It is selective for binding to Ca(II), which it prefers 1000 times over Mg(II)[22] (see Table 15 for log K_1 values for the EGTA analog). EGTA has an ability to form complexes with a wide variety of metal ions.[25] Thus, FURA-2 was initially used to study the fluorescent properties with a wide variety of metal ions, specifically Ca^{2+}, Zn^{2+}, Cu^{2+}, Ni^{2+}, and Bi^{3+}. This was carried out to provide a preliminary indication as to which metal ions produced complexes that fluoresced most intensely and which complexes were quenched. The intention here was to establish trends of CHEF effects across the periodic table, information which is currently lacking. Research has been focused on metal ions of importance in biology, such as Mg(II), Ca(II), and Zn(II),[10-13] or of interest in photochemistry (Ru(II) and Cu(I)). A few studies have been focused on testing the Energy Gap rule, with, for example, Re complexes.[29] There has been no attempt to examine in a systematic way which metal ions in the periodic table are able to induce a CHEF effect with a common ligand.

Results for the CHEF effect of Ca(II), Ni(II), Cu(II), Zn(II) and Bi(III) are summarized in Fig. 20. It is seen that Ni(II) and Cu(II), which are paramagnetic ions, quench the fluorescence of FURA-2 very strongly. Zn(II) also does not produce a strong CHEF effect, which almost certainly relates to the fact that Zn(II) is reluctant to adopt an eight-coordinate structure, but prefers to be 4,5,or 6 coordinate. This can leave two N or O donor atoms on FURA-2 non-coordinated to the Zn(II), and therefore free to quench the fluorescence of FURA-2. The point of interest here is the small CHEF effect of

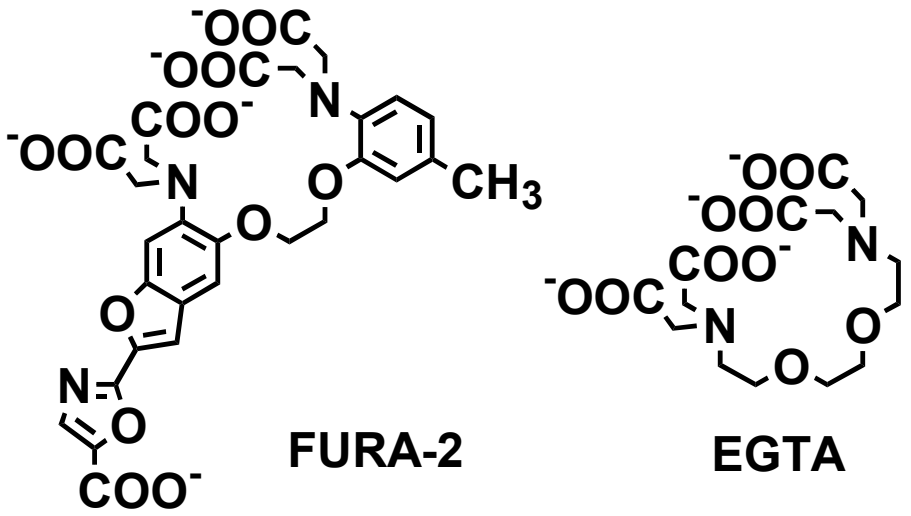

Figure 19. Structure of FURA-2, an EGTA analog, along with structure of EGTA. The negatively charged oxygens of the ester groups, along with the ether oxygens bridging between aromatic groups all can chelate a metal ion. These charged ester oxygens can be protonated, which limits complexation of other metal ions.

Table 15. Some binding constants for EGTA with metals of interest, taken from the NIST database[25]. All are at 25°C, in 0.1 *M* ionic strength solution.

Metal ion	log K with EGTA
Ca (II)	10.8
Zn (II)	12.2
Ni (II)	13.5
Cu (II)	17.7
Bi (III)	23.8

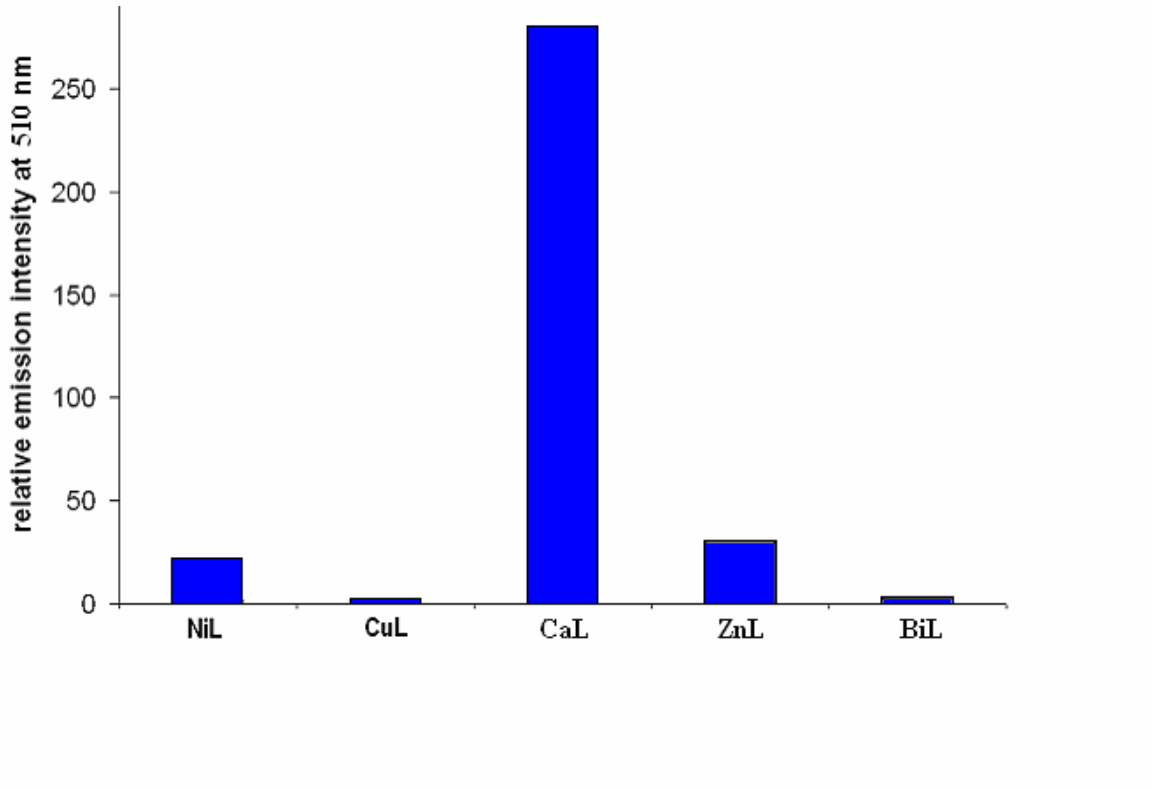

Figure 20. Relative emission intensity of metal complexes with FURA-2 at 510 nm. The excitation wavelength is at 350nm. L represents FURA-2. The concentration of all the metal complexes is 10^{-5} M.

Bi(III) with FURA-2. Several factors might contribute to this effect. Initially, one notes that the CHEF effect is smaller in Cd(II) complexes than in analogous Zn(II) complexes. In addition, complexes of Hg(II) do not appear to display a CHEF effect. This is probably a manifestation of Energy Gap effects, that orbitals in the heavier metals are getting too close to the π^* orbitals of the ligands. Bi(III) is a heavy metal ion, with large relativistic effects.[30] One might thus expect energy gap effects to diminish the fluorescence of Bi(III) complexes. A second contributing factor here might be the lone pair on Bi(III). The Bi(III) ion, like Pb(II), has a lone pair of electrons occupying the *6s* orbital. These electrons may be able to quench fluorescence in the same way that lone pairs on N-donors or O-donors on ligand can quench fluorescence.

The fluorescence produced by Ca^{2+} shows a very strong CHEF effect. This is because Ca^{2+} is readily able[31] to produce a coordination number of 8 required for coordinating all the donor atoms on FURA-2. It should be noted that preliminary work that was carried out on the Pb(II) complex of FURA-2 suggested that this would also not show a CHEF effect. This was in spite of the fact that Pb(II) is even larger than Ca(II), and readily assumes an eight coordinate geometry. The reasons for this are presumably similar to why Bi(III) does not produce a CHEF effect, namely, the position of Pb(II) as a heavy element in the periodic Table, and the fact that it possesses a lone pair of electrons.[30]

Fluorescence study of Ni(II)-terpyridine and Zn(II)-terpyridine

The aim in this part of the work was to see if the $[Ni(terpy)(H_2O)_3]^{2+}$ complex could be used to detect small ligands such as CN^- ion by fluorescence. The idea here, as discussed in the introduction, was to see whether change of spin state on coordination of CN^- to the complex would induce a strong increase in fluorescence:

$$[Ni(terpy)(H_2O)_3]^{2+} + CN^- \quad \leftrightarrows \quad [Ni(terpy)CN]^+ \quad + \quad 3H_2O$$

high-spin — low-spin

non-fluorescent — fluorescent

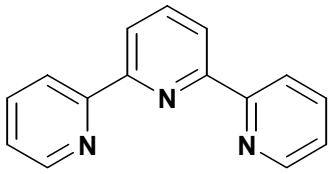

terpy

To date, no examples have been reported of this type of effect, which would represent a totally novel type of sensor for small molecules. In addition to the Ni(II)-terpyridine complex, the Zn(II)-terpyridine complex was studied for comparison purposes, since Zn(II) is capable of inducing a strong CHEF effect. Terpyridine on its own in acidic media does fluoresce when exposed to its optimum excitation wavelength of 360 nm. Ni(II)-terpyridine as a 1:1 complex did not exhibit fluorescence. Figure 21 shows the emission spectra for terpyridine alone, Zn(II)-terpyridine, and Ni(II)-terpyridine, all at a low pH.

Fluorescence studies for terpyridine complexes were also carried out in more basic aqueous media. Due to the relative insolubility of the terpyridine in water, an acidic solution of terpyridine was initially made up, followed by a pH adjustment with 1.00 *M* NaOH solution.

Secondary ligand addition to the Ni(II) / terpyridine complex

Addition of a secondary ligand to the Ni(II)-terpyridine complex was attempted in order to restore fluorescence. NaCN solution was added to the 1:1 Ni(II)-terpyridine aqueous complex and an emission spectrum was obtained. Because the pK_a for HCN is 9.2, the overall pH of the solution had to be above the pK_a.[25] Figure 22 shows the results of adding increasing molar ratios of NaCN to Ni(II)-terpyridine in aqueous solution with pH values above nine. The resulting increase in fluorescence emission suggested that we might have achieved our aim of using the Ni(II)/terpy complex as a sensor for CN-. All other possible species in solution were checked to see if they could account for the observed increase in fluorescence. The species checked were $Ni(CN)_4^{2-}$, Ni(tpy), and $Ni(tpy)_2$, as well as free terpy A solution consisting of solely $Ni(CN)_4^{2-}$ was excited at 360 nm and resulted in no emission. Emission spectra were then generated for a $Ni(tpy)_2$ solution, which showed no evidence of fluorescence. A troubling finding was that the fluorescence spectrum of terpy itself was found to be identical to the set of spectra found in Figure 22, as seen in Figure 23. Further studies showed that there was a slow decrease with time of the intensity of the fluorescence spectra obtained by adding CN^- to the Ni(II)/terpy complex. This suggested that the correct explanation for the set of spectra seen in Figure 22 was as follows:

$$\underset{\text{non-fluorescent}}{[Ni(terpy)(H_2O)_3]^{2+}} + 4\,CN^- \xrightarrow{\text{fast}} [Ni(CN)_4]^{2-} + \underset{\text{fluorescent}}{\text{terpy}} \qquad [11]$$

$$[Ni(terpy)(H_2O)_3]^{2+} + \text{terpy} \xrightarrow{\text{slow}} \underset{\text{non-fluorescent}}{[Ni(terpy)_2]^{2+}} \qquad [12]$$

The results in Figure 22 are thus explained in terms of initial displacement of terpy from Ni(II) by CN^- to form the $Ni(CN)_4^{2-}$ complex. The displaced terpy is fluorescent, and it is this fluorescence that gives the impression of enhanced fluorescence due to a mixed Ni(II)/terpy/CN^- complex. The observed fluorescence slowly fades with time because of slow reaction to form the Ni(II)/bis-terpy complex, which is not fluorescent. This mechanism has been supported by the crystal structure shown in Figure 16. These crystals were grown from a 1:1:1 mixture of Ni(II), terpy, and CN^-. It is seen that the complex obtained is not the mixed ligand $[Ni(terpy)CN]^+$ complex, but rather the $[Ni(terpy)_2][Ni(CN)_4]$ complex, supporting the idea that the actual source of the fluorescence seen in Figure 22 is the disproportionation reaction [11] above.

Other secondary N-donor ligands with Ni(II) / terpyridine

Fluorescence was further explored with the Ni(II)-terpyridine system, using alternative secondary nitrogen donor ligands such as pyridine and azide. Figure 24 and figure 25 depict the emission spectra of Ni(II)-terpyridine, adding pyridine and azide, respectively. Fluorescence was increased by 75% upon addition of 50 times more pyridine to 1:1 Ni(II)-terpyridine, and decreased by 25% after a 10-fold increase in [azide] to the 1:1 Ni(II)-terpyridine complex. All of the above-described solutions were adjusted to a pH between 10 and 10.5, to keep the solution conditions identical to those employing cyanide as a secondary ligand. The modest increase in fluorescence produced by pyridine suggests that further investigation of the Ni(II)/terpy/pyridine system might be worthwhile.

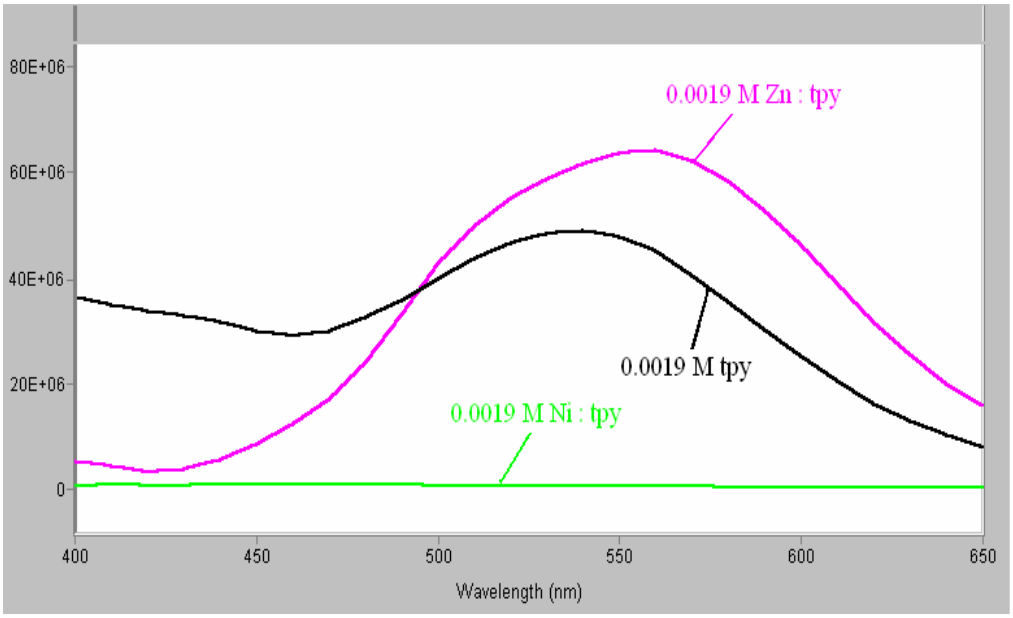

Figure 21. Fluorescent emission spectra for terpyridine (tpy), Zn(II)-terpyridine, and Ni(II)-terpyridine, all at low pH values (1.6-1.9). Note the CHEF effect of the Zn(II)-tpy complex, as compared to the tpy on its own. The Ni(II)-tpy complex exhibits no fluorescence emission.

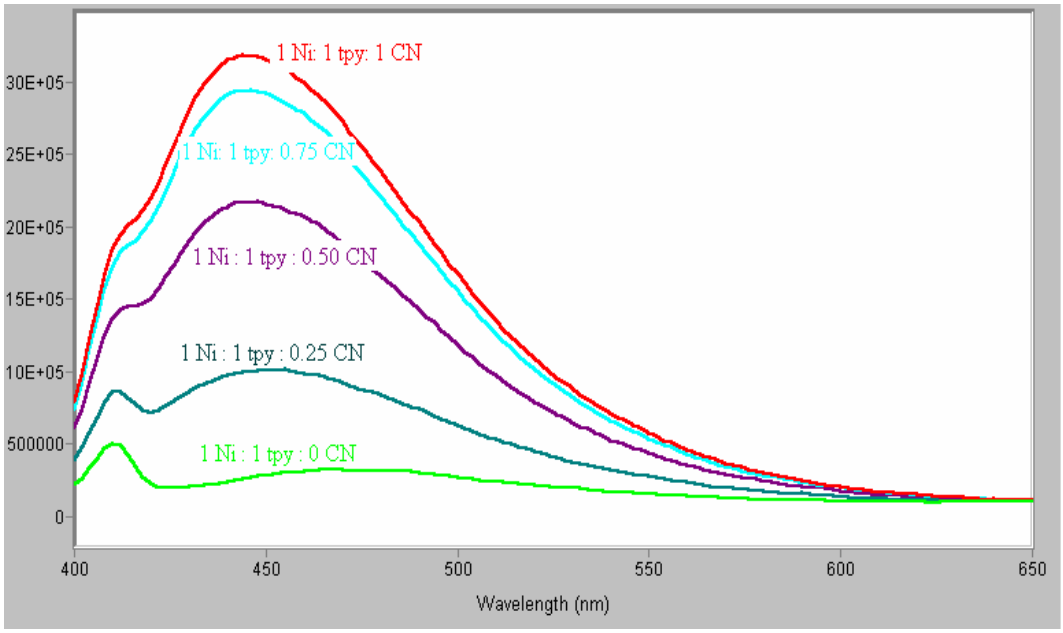

Figure 22. Fluorescent emission spectra for Ni(II)-terpyridine (tpy), with increasing CN^- molar ratios. The pH values for all of these solutions were between 9 and 10.6. The concentrations of the Ni(II) and the terpyridine were 0.0019 M. The diagram suggests that this system might be used as a sensor for CN^-, since fluorescence increases with increasing CN^- concentration. However, as discussed in the text, the actual reactions occurring in the system are more complex, and may not lead to a practical sensor system.

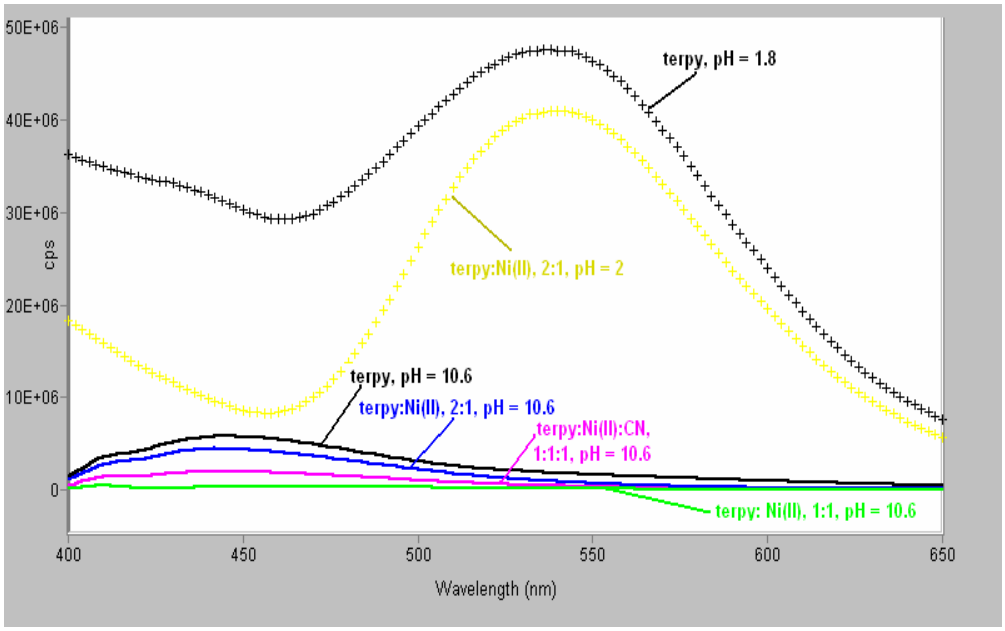

Figure 23. Emission spectra for species containing Ni(II), tpy, and CN^-. The excitation wavelength used to generate each spectrum was 360 nm. Concentrations of reactants were made as 0.00095 *M* for the molar ratio of 1, and 0.0019 *M* for the molar ratio of 2. Note that the emission spectrum of terpy (black line) at pH 10.6 is very similar to that of a 1:1:1 Ni(II)/terpy/CN- mixture at the same pH.

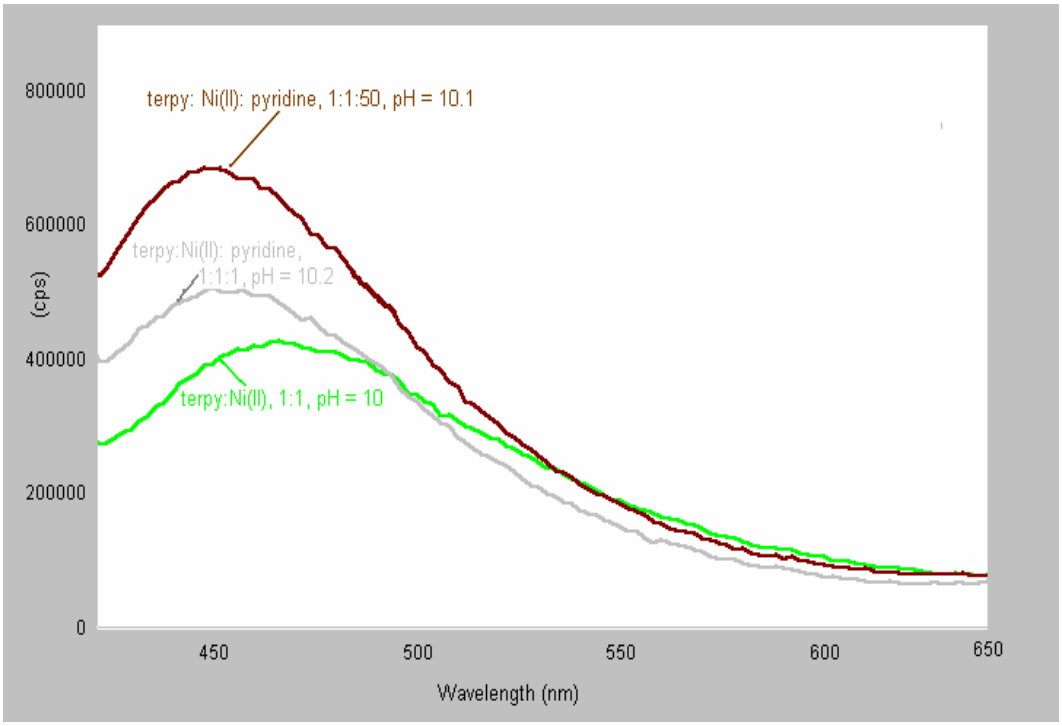

Figure 24. Emission spectra for Ni-tpy with increasing pyridine, at pH values > 10. Note the increase in fluorescence on adding 50:1 pyridine.

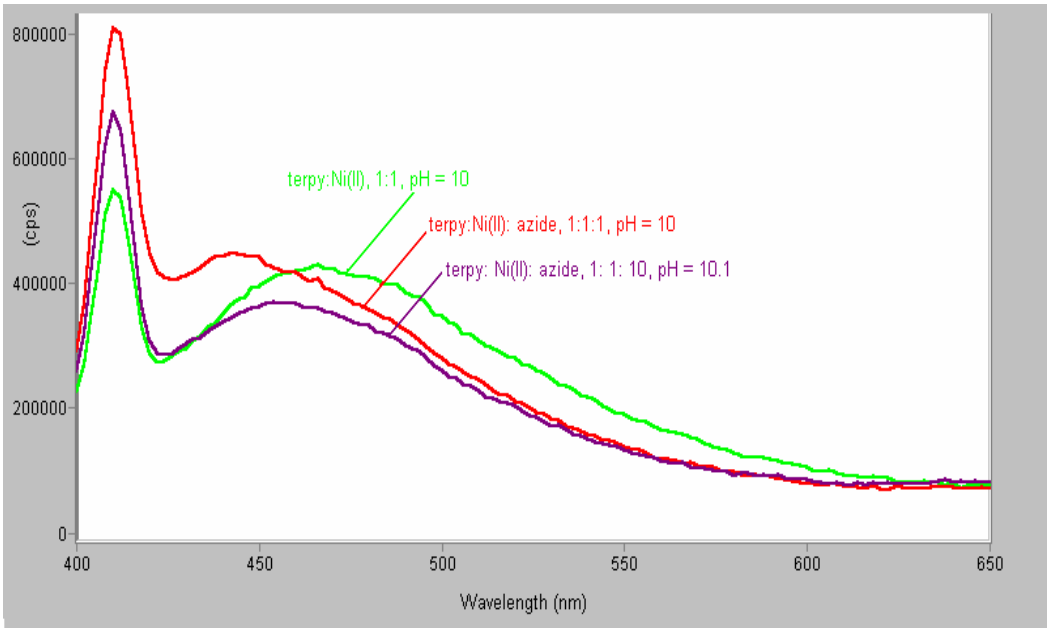

Figure 25. Ni-tpy-azide fluorescence emission spectra, with increasing [azide]. All pH values are > 10.

Effects of pH on the terpyridine system: adding NaOH to the known fluorescing complex Zn(II)-terpy.

As discussed later, it appeared that one possible reason for the inability of a 1:1:1 Ni(II)/terpy/CN^- system to form a mixed ligand complex was the high acidity of water molecules coordinated to Ni(II). In order to study such an effect in Zn(II), which might be expected to show similarly high acidity, the effects of pH on fluorescence emission of the Zn-tpy system was explored. Based on Figure 26(a), the Ni(II)-terpyridine-CN^- species experience a decrease in fluorescence when the pH is increased to 10. However, this is necessary because of the high pKa value for HCN of 9.2. As is evident in Figure 26, there is a CHEF effect occurring at 420 nm as pH is increased. This is due to the replacement of the protonated terpyridine at lower pH values with Zn(II) at higher pH values, and ultimately deprotonation of the waters of hydration bound to the Zn-tpy complex. One sees in Figure 26(a) that at pH 1.6 there is intense fluorescence with a peak at about 545 nm. This is due to the presence of protonated forms of terpy. At pH 5.4 the peak has shifted to 479 nm, which is fluorescence due to the Zn(II)/terpy complex. A further shift occurs at higher pH, with a peak at 425 nm, which is assigned to the deprotonated complex $[Zn(terpy)OH]^+$. The excitation wavelength was set at the same value throughout the experiments, at 360 nm.

As seen in Figure 26(b), the midpoint in the transition from the [Zn(terpy)H2O]2+ complex to the [Zn(terpy)OH]+ complex, as indicated by the fluorescence spectra, occurs at about pH 7.9. This would make the complex $[Zn(terpy)H_2O]^{2+}$ much more acidic than the Zn^{2+} aquo ion, which is only deprotonated at pH 9.4. This result has some bearing on the unusual acidity of the Ni(II)/terpy complex discussed below.

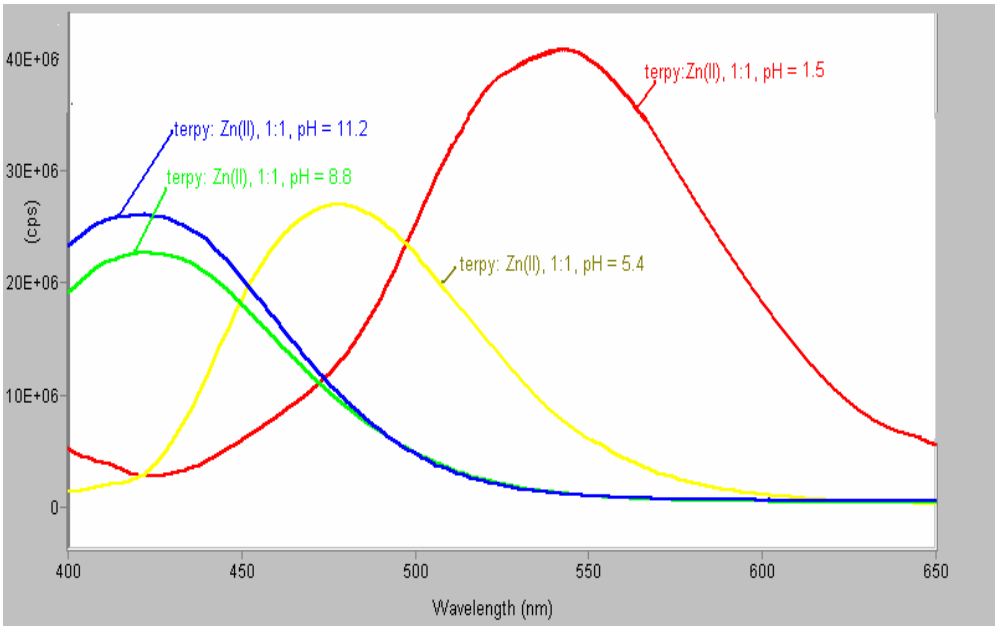

Figure 26(a). Emission spectra for the 1:1 Zn-tpy complex as a function of increasing pH (increasing $[OH^-]$). The fluorescence at pH 1.5 (red spectrum) is that for protonated terpy species, since the Zn(II)/terpy complexes will have been broken up. The spectrum at pH 5.4 (yellow) is that for the Zn(II) mono-terpy complex. The spectra at pH 8.8 (green) and 11.2 (blue) are for the deprotonated complex, probably $[Zn(terpy)(OH)]^+$.

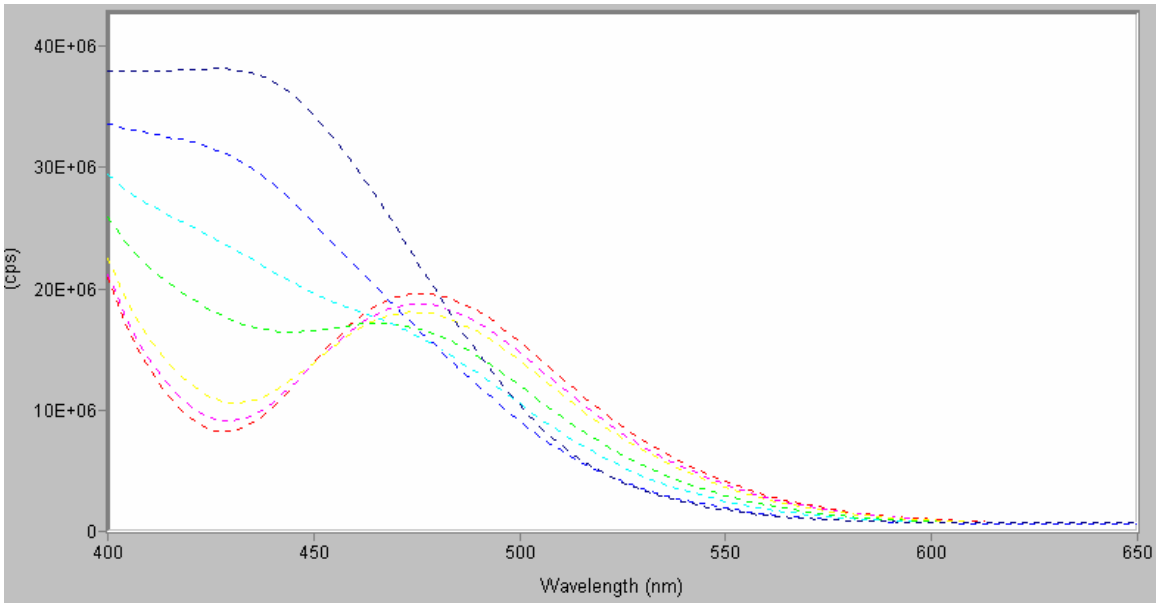

Figure 26(b). Emission spectra for the 1:1 Zn(II)/terpy complex between pH 7 and 9. The spectra are at the following pH values: pink, 7.12; yellow, 7.38; green, 7.71; turquoise, 7.85; blue, 8.01; purple, 8.30; red, 8.51. The midpoint of the set of spectra is at about pH 7.9, suggesting a rather high acidity for the complex $[Zn(terpy)H_2O]^{2+}$. The breakdown of the isosbestic point that initially appears at 460 nm, at higher pH values, may be due to the formation of species such as $[Zn(terpy)(OH)_2]$

Voltammetric study of the acidity of the nickel(II) mono-terpyridine complex

It appeared from the work with Zn(II) that one possible reason why the Ni(II)/terpy complex was so reluctant to add a CN^- to form the mixed ligand complex was that the Ni(II)/terpy complex might show high acidity, and be deprotonated at pH 10 where the fluorescence experiments were carried out. The coordinated hydroxide ion might thus compete effectively with CN^- for binding to the Ni(II), and prevent it from binding to the Ni(II)/terpy complex. Voltammetric techniques were employed to determine the binding of hydroxide to the Ni(II)/terpy complex.. All titrations were carried out in a background electrolyte consisting of 0.01M HNO_3 and 0.49M $NaNO_3$. A set of data of *E* versus volume of the added 0.01 M NaOH / 0.49 M $NaNO_3$ solution was collected by titration of 5×10^{-5} M Ni^{2+}/ terpyridine with NaOH. An example of a voltammogram, recorded at pH 3.075, for the Ni(II)/terpy system is seen in Figure 27. The figure shows a peak at -0.90 V, which is that observed for the Ni^{2+} aquo ion. A peak at -1.17 V is not present in terpy alone, and is assigned to the Ni(II)/terpy complex. Further peaks at -1.27 V and -1.33 V are assigned by comparison with the voltammogram for terpy alone at the same pH to reduction of pyridyl groups as in:

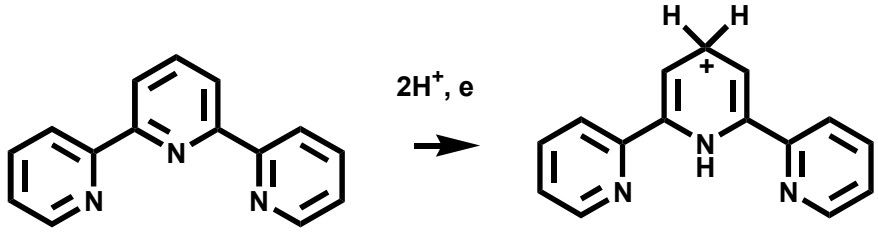

The resulting voltammetric peak positions due to the Ni-terpyridine complex were then measured as a function of increasing pH. The labile peaks changed position as the pH of the solution was increased towards a more negative, less reducible potential. Figure 28

shows the peak position versus pH plot for the Ni(II)-terpyridine complex. It is seen that the peak shifts to more negative potential with increasing pH. There are two clear inflections in the shift. The first inflection occurs at pH 8.3. This type of inflection corresponds[32] to deprotonation of solution species, and in this case this is reasonably assigned to the deprotonation of the complex:

$$[Ni(terpy)(H_2O)_3]^{2+} + OH^- \leftrightarrows [Ni(terpy)(H_2O)_2OH]^+$$

The pH at which the inflection occurs is the pK_a of the complex, in this case 8.3. The second inflection at pH 10.1 corresponds to the second deprotonation:

$$[Ni(terpy)(H_2O)_2OH]^+ + OH^- \leftrightarrows [Ni(terpy)(H_2O)(OH)_2]$$

pK_a of terpyridine with Ni(II)

At an ionic strength of 0.5 as used here, pK_w is 13.74, which means that log $K_1(OH^-)$ for the Ni(II)/terpy complex is 13.74 – 8.3 = 5.44. This is considerably more acidic than the Ni^{2+} aquo ion, for which log $K_1(OH^-)$ is 3.7. This increase in acidity may relate to the steric properties of the terpy ligand when it coordinates to a small metal ion such as Ni(II). The two *ortho* hydrogens on the terpy ligand that are adjacent to the coordinated water molecule (Figure 29) provide a hydrophobic environment for that water molecule. Deprotonation reduces the positive charge on the water molecule, and so lowers the pKa of the complex, as was found here by voltammetric titration.

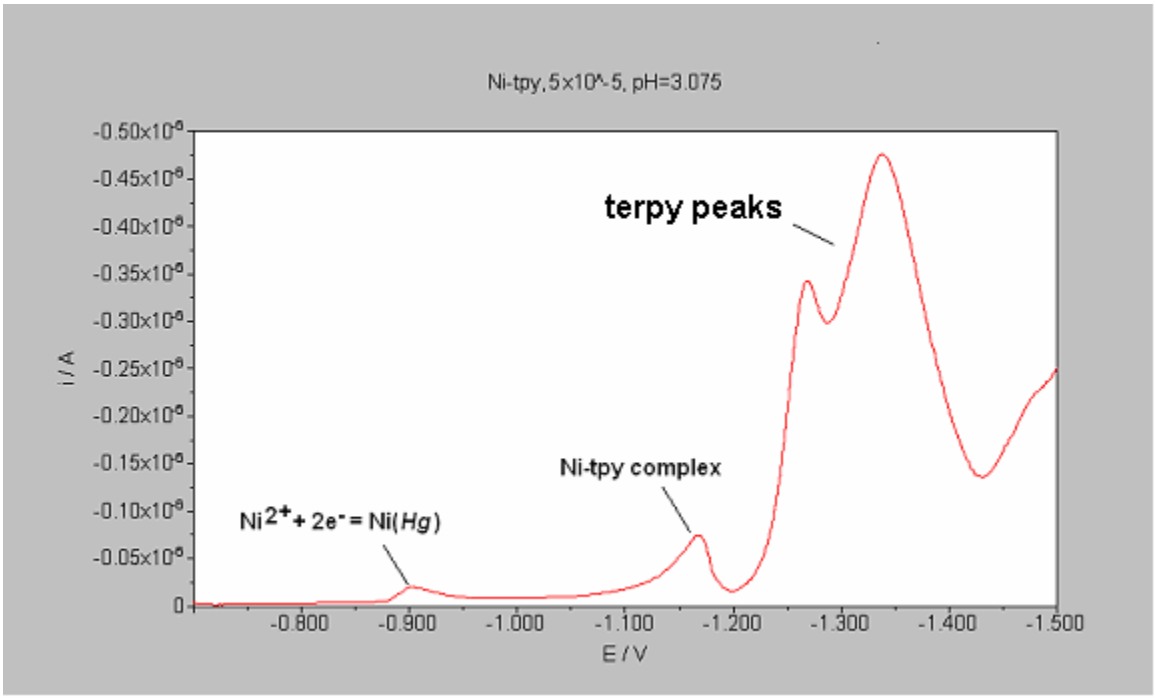

Figure 27. Voltammogram for 5 x 10^{-5} *M* Ni(II)-terpyridine at pH =3.075. Note the peak position for the Ni(II)-terpyridine complex, -1.17 V, and the Ni^{2+} aquo ion at -0.9 V. The two peaks at -1.27 V and -1.33 V are present in terpy on its own at this pH, and are assigned to ligand reduction potentials as discussed in the text.

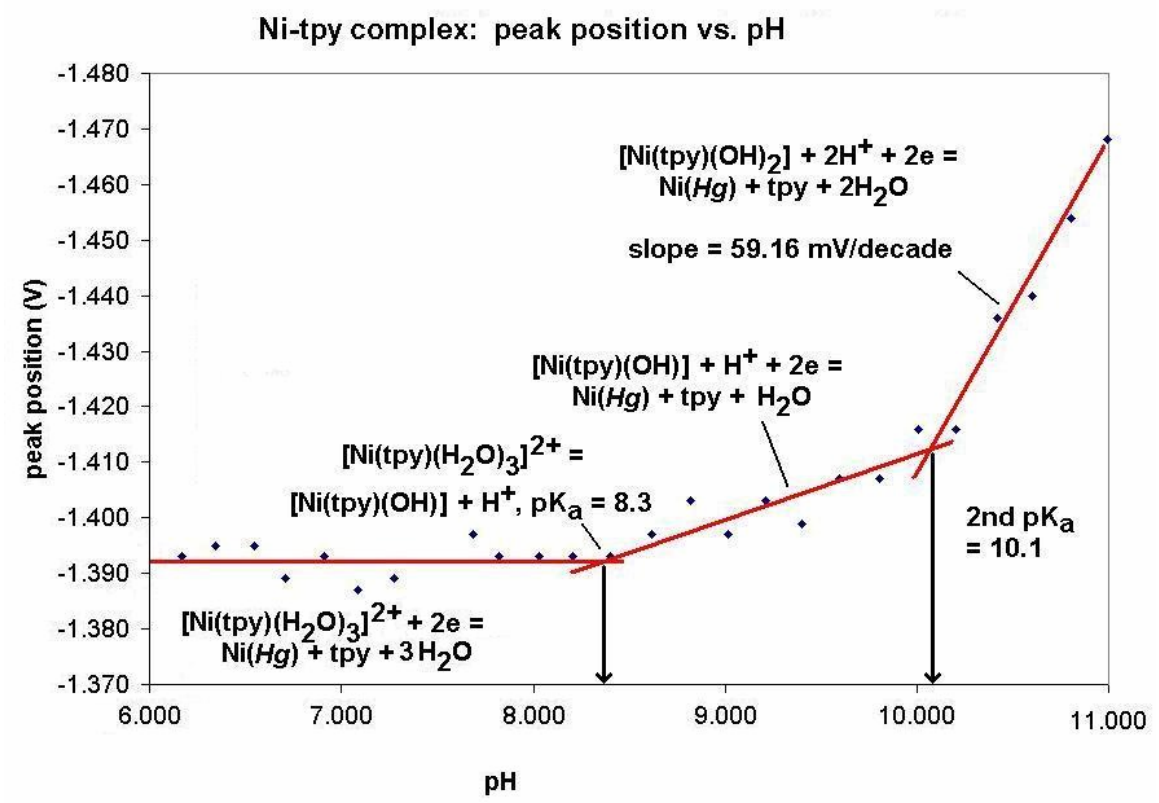

Figure 28. Plot of peak position versus pH for the Ni(II)-terpyridine complex. The three regions of proton activity are denoted, as well as their respective equations.

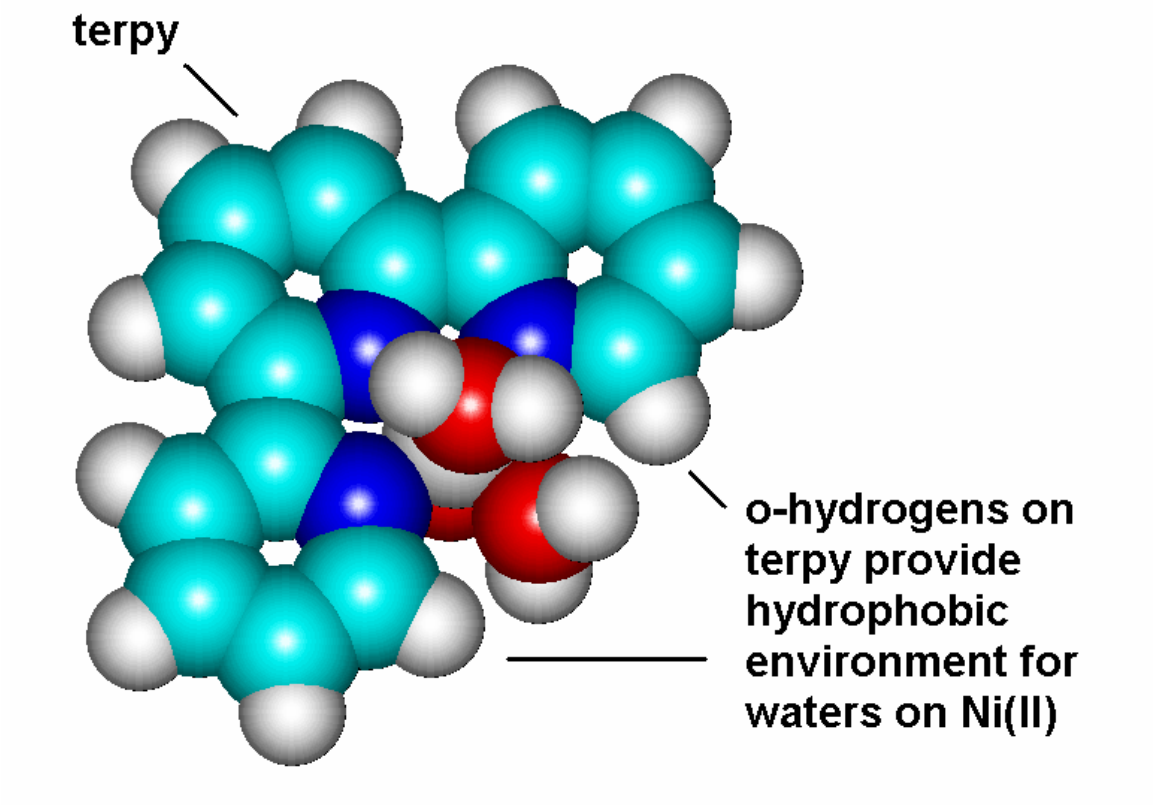

Figure 29. The $[Ni(terpy)(H_2O)_3]^{2+}$ complex, showing how the ortho hydrogens on the terpy ligand surround one water molecule coordinated to Ni(II). This more hydrophobic environment encourages loss of a proton to reduce the overall charge on the complex, and causes a significantly lower pK_a for the complex. Structure of the complex was generated by molecular mechanics calculation using the program HyperChem[24].

Table 16. Data points for plot of Ni(II)-terpyridine versus pH (see Figure 28).

pH	peak position
5.490	-1.379
5.657	-1.383
5.772	-1.383
5.943	-1.397
6.166	-1.393
6.344	-1.395
6.543	-1.395
6.706	-1.389
6.910	-1.393
7.084	-1.387
7.277	-1.389
7.686	-1.397
7.824	-1.393
8.029	-1.393
8.208	-1.393
8.400	-1.393
8.620	-1.397
8.821	-1.403
9.019	-1.397
9.209	-1.403
9.400	-1.399
9.593	-1.407
9.803	-1.407
10.011	-1.416
10.206	-1.416
10.417	-1.436
10.605	-1.440
10.802	-1.454
10.990	-1.468

CONCLUSIONS

One of the initial goals of this research was induction of fluorescence by secondary ligands in solution. The high-spin Ni(II) / terpyridine complex was studied extensively due to the tendency of the d_8 Ni^{2+} ion to quench fluorescence. It was believed to be possible to induce fluorescence by addition of a secondary ligand high enough in the spectrochemical series[8] such as to close in on the energy gap by lowering the energy of the e_g degenerate orbitals, giving rise to a low spin complex that could fluoresce. What actually occurred was a disproportionation reaction governed by the fast conversion of Ni(II) / terpy to $Ni(CN)_4^{2-}$ upon addition of an equimolar amount of CN^-. Much slower was the formation of $[Ni(terpy)_2]$, which exhibited fluorescence as shown. The crystal structure provided additional proof of the presence of the above-mentioned species. A voltammetric study was conducted with Ni(II) / terpy to aid in the determination of the complex peak. The first pKa found for the $[Ni(II)(terpy)(H_2O)_3]^{2+}$ complex, indicative of a deprotonation of one of the waters of hydration, is 8.3. The second pKa was found to be 10.1 by this method. Both of these are much more acidic than the first and second pKa values for the Ni(II) aquoion, which are reported to be 9 and 12, respectively.[25]

The formation constant of In(III) with 1,10-phenanthroline was investigated via voltammetric titration as a function of pH. Voltammetric peaks were assigned by careful comparison of In(III)/ 1,10-phen voltammograms with those for 1,10-phen alone. Log K_1 was calculated to be 6.65 by this method. ^1H NMR was also used to determine the binding constant of In^{3+} with 1,10-phen as a validation to the voltammetric experiments. Chemical shifts of protons were tracked as a function of pH, and n bar was calculated.

From this, the log K_1 was calculated to be 6.85. The log K_1 value found experimentally using voltammetric techniques is lower than expected most likely due to the inherent difficulty in the initial E_0 determination due to the weak signal exhibited by the In^{3+} aquo ion under voltammetric conditions.

REFERENCES

1. Skoog, D.A., Holler, F.J., Nieman, T.A., Principles of Instrumental Analysis, Harcourt College Publishers, 1984.
2. Demas, J.N., DeGraff, B.A., *J. Chem. Educ.,* 1997, **74**, 691.
3. Lakowicz, J.R., Principles of Fluorescence Spectroscopy, Plenum Press, New York and London, 1983.
4. Lees, Alistair J., *Chem. Rev.*, 1987, **87**, 711-743.
5. McMurry, J., Organic Chemistry, Brooks/Cole, Belmont, CA, 2004.
6. Lakowicz, J.R. Principles of Fluorescence Spectroscopy- Second Edition, Plenum Press, New York and London, 1999.
7. McMillin, D.R., McNett, K.M, *Chem. Rev.*, 1998, **98**, 1201.
8. Sakaki, S., Mizutani, H., Kase, Y. *Inorg. Chem.*, 1992, **31**, 4575.
9. Everly, M. Ziessel, R., Suffert, J., McMillin, D. *Inorg. Chem.,* 1991, **30**, 559.
10. Walkup, G. K., Burdette, S. C., Lippard, S. J and Tsien, R. Y. *J. Am. Chem. Soc.,* 2000, **122**, 5644-5645.
11. Kimura, E. and Aoki, S. *BioMetals*, 2001, **14**, 191-204.
12. a) Burdette, S.C., and Lippard, S.J., *Coord. Chem. Rev.*, 2001, **216**, 333.
    b) Burdette, S.C., and Lippard, S.J., *Proc. Natl. Acad. Sci.*, 2003, **100**, 3605.
13. Burdette, S. C., Walkup, G. K., Spingler, B., Tsien, R. Y. and Lippard, S. J. *J. Amer. Chem. Soc.,* 2001, **123**, 7831.
14. Gan, W. Synthesis and analysis of DQPMA and DQPEA: Versatile Zn(II) fluorescent detectors, UNC-Wilmington, 2004.

15. Goodwin, K.V., McMillan, D.R., *Inorg. Chem.,* 1987, **26**, 875-877.

16. Martell A.E, Hancock R.D., Metal Complexes in Aqueous Solutions., Plenum Press, New York and London, 1996.

17. Hancock, R.D., Martell, A.E., *Chem. Rev*.,1989, **89**, 1875.

18. Thom, V.J., Fox, C.C., Boeyens, J.C.A., Hancock, R.D. *J. Amer. Chem. Soc*., 1984, **106**, 5947.

19. Martell, A.E., Smith, R.M., Critical Stability Constants, Plenum, New York, **Vols.1-6,** 1974, 1975, 1977, 1978, 1982, 1986.

20. Hancock, R.D., Martell, A.E., Metal Complexes in Aqueous Solutions, Plenum Press, New York and London, 1996.

21. Housecroft, C.E., Sharpe, A.G., Inorganic Chemistry, Prentice Hall, Harlow, England, 2001.

22. Bond, A.M., Modern Polarographic Methods in Analytical Chemistry, Marcel Dekker, Inc., New York, 1980.

23. Silverstein, R.C., Webster, F.X., Spectrometric Identification of Organic Compounds, 6th ed., John Wiley & Sons, New York, 1998.

24. HyperChem program, version 7.5, Hypercube, Inc., 419 Philip Street, Waterloo, Ontario, N2L 3X2, Canada.

25. Martell, A. E.; Smith, R. M. *Critical Stability Constant Database*, 46, National Institute of Science and Technology (NIST), Gaithersburg, MD, USA, 2003.

26. Hancock, R.D., Cukrowski, I., and Mashishi, J. "The Affinity of Bismuth(III) for Nitrogen-donor ligands", *J. Chem. Soc., Dalton Trans.*, 2895-2899 (**1993**).

27. Hancock, R.D., Cukrowski, I., Cukrowska, E., Antunes, I. Mashishi, J., and Brown, K. "Complexation of Bismuth (III) by Nitrogen Donor Ligands. A Voltammetric Study", *Polyhedron*, Vol. 14, p 1699 (**1995**).

28. Kulba, F. Ya., Makashev, Yu. A., and Fedyaev, N. I. *Russ. J. Inorg. Chem.*, 17, 188 (1972).

29. Caspar, J., and Meyer, T. J. Application of the Energy Gap Law to non-radiative excited state decay, *J. Phys. Chem*., Vol. 87, pp 952-957 (1983).

30. J. M. Harrington, S. B. Jones, P. H. White, and R. D. Hancock, "The Possible Role of Relativistic Effects in the Plasticity of the Coordination Geometry of Cadmium(II). A Voltammetric study of the Stability of the Complexes of Cadmium(II) with 12-crown-4, 15-crown-5 and 18-crown-6 in Aqueous Solution, and the Structures of [Cd(benzo-18-crown-6)$(NCS)_2$] and [K(18-crown-6)][Cd$(SCN)_3$]", *Inorg. Chem.*, Vol. 43, 4456-4463 (**2004**).

31. R. D. Hancock, C. J. Siddons, K. A. Oscarson, and J. H. Reibenspies, "The Structure of the Eleven-Coordinate Barium Complex of the Pendant Donor Macrocycle 1,4,7,10-tetrakis(carbamoylmethyl)-1,4,7,10-tetraazacyclododecane. An analysis of the Coordination Numbers of Barium(II) in its complexes", *Inorg. Chim. Acta*, Vol. 357, pp. 723-727 (**2004**).

32. R. Luckay, I. Cukrowski, J. Mashishi, J. H. Reibenspies, A. H. Bond, R. D. Rogers, and R. D. Hancock, "Synthesis, Stability, and Structure of the Complex of Bismuth(III) with the Nitrogen Donor Macrocycle Cyclen (1,4,7,10-tetraazacyclododecane). The role of the lone pair on Bismuth(III) and Lead(II) in

determining Coordination Chemistry", *J. Chem. Soc., Dalton Trans.*, pp. 901-908 (**1997**).